PERGAMON

International Journal of Solids and Structures 36 (1999) 3131–3169

INTERNATIONAL JOURNAL OF SOLIDS and STRUCTURES

Matrix crack initiation and progression in composite laminates subjected to bending and extension

Erik Adolfsson*, Peter Gudmundson

Department of Solid Mechanics, Royal Institute of Technology, S-100 44 Stockholm, Sweden

Received 12 November 1996; in revised form 10 April 1998

Abstract

An experimental investigation of matrix crack initiation and progression in glass/epoxy laminates of different stacking sequences is presented. The laminates have been loaded in extension and bending, and the degree of damage as function of the load has been recorded. The changes in certain elastic properties caused by the damage were also measured, and are compared to results from a previously developed approximate analytic model. An energy release rate resistance curve is adopted in an attempt to describe the initiation and progression of matrix cracks in the laminates. The amount of cracking is also viewed in relation to the strain transverse to the fibres in the ply under consideration, and the ply stresses at the onset of cracking are calculated. The different damage evolution criteria are compared to the experimental results, and their validity and reliability are discussed. By use of the ply strain transverse to the fibres as a critical parameter for damage evolution, the load–deformation curves of the tested laminates are simulated taking damage progression into account.

1. Introduction

The mechanical properties of advanced polymer based fibre composites have been of interest to the scientific community for a considerable period of time. An issue of particular concern is the degraded properties of composites containing different types of damage. A laminated composite in service often exhibits several distinguishing modes of deterioration preceding the final fracture. Such characteristic damage modes are matrix cracking, fibre fracture, fibre-matrix debonding and delamination. A basic goal of the ongoing research on composite laminates is the construction of damage initiation and progression criteria. Such criteria could be used in combination with information of the stress–strain relation for a certain damage state to derive a constitutive equation taking damage evolution into account. Estimations of the damage resulting from a certain load history may allow for longer service inspection intervals for composite structures.

* Corresponding author. Fax: 00 46 8 411 24 18; E-mail: erik@hallf.kth.se

0020–7683/99/$ - see front matter
PII: S0020–7683(98)00142–5

Of the damage categories mentioned above, the first to appear in a composite laminate under mechanical and thermal loading is often matrix cracking. The matrix cracks seldom cause complete laminate failure, but can considerably impair the performance of the composite. The decrease in stiffness can, however, be lifetime limiting in certain stiffness dependent applications, see Prosser et al. (1995). Matrix cracks have also, in addition, shown to promote secondary damage modes in composites. Jamison and Reifsnider (1982) reported on the influence of matrix cracks on fibre fracture in adjacent plies. Matrix crack induced delaminations have also been investigated, see e.g. Altus and Ishai (1990), Jen and Sun (1990), Armarinos et al. (1991) and O'Brien (1993). The coupling effects between matrix cracks and delaminations were further investigated in the works by Eggers et al. (1994) and by Ogihara and Takeda (1995). The importance of taking into account the coupling between different types of damage was stressed by Nairn and Hu (1994). Prior to doing so, however, it is desirable to establish a thorough understanding of the separate damage modes.

The problem of predicting the behaviour of a composite laminate in service may be partitioned into two sub-problems. One of these, and usually the first one that is solved, is the determination of the constitutive relation of a laminate with a certain damage distribution. The other problem that needs attention in order to acquire a damage dependent constitutive law is matrix crack initiation and progression.

The reduction of the thermoelastic properties of composite laminates with matrix cracks has attracted much attention from researchers for a period of time. Aveston and Kelly (1973) along with Hahn and Tsai (1974) were amongst the first researchers to account for a stiffness degradation related to matrix cracks in advanced composite laminates. The methods for prediction of stiffness degradation which have since then emerged form the collected scientific efforts range from the simple ply-discount method adopted by for example Sendeckyj et al. (1974) to more sophisticated methods using a minimum of approximations.

The shear-lag method appropriated by Reifsnider (1977) offers a relatively uncomplicated way of calculating the reduced stiffnesses of cracked laminates. The load transfer between neighbouring plies is assumed to take place in a so-called shear layer of a generally unknown thickness. There is in general a need for experimental data in order to apply the shear lag concept. Hashin (1985, 1987, 1988) used the principle of minimum complementary energy to derive estimates of the thermoelastic properties of cracked laminates. Self consistent approximations were applied by Laws et al. (1983) and Dvorak et al. (1985) to calculate the stiffnesses and thermal expansion coefficients of laminates with matrix cracks.

The majority of the developed methods for prediction of the reduced properties of cracked laminates are applicable only to cross-ply laminates, which is evident in the review presented by Abrate (1991). Gudmundson and Zang (1993) developed a way of predicting the reduced extensional thermoelastic properties of a general three-dimensional laminate with an arbitrary distribution of matrix cracks. This method was later extended to enable calculation of the reduced flexural and extensional thermoelastic properties of laminated plates and shells in the work by Adolfsson and Gudmundson (1997).

For a successful treatment of the damage evolution problem, both the method for calculation of the reduced thermoelastic quantities of the damaged laminate and the matrix crack initiation and progression criterion must be reliable. A number of approaches for the prediction of matrix crack initiation and progression can be found in the literature. Damage evolution criteria may be

of critical stress or critical strain type, or may be formulated in terms of stress intensity factors or energy release rates.

Energy release rate criteria for onset and progressive growth of matrix cracks have been applied by numerous authors in the recent decades. An early discussion of cracking in uniaxially reinforced composites in terms of critical energies is found in the work by Aveston and Kelly (1973). The energy concept for crack formation was further treated by Parvizi et al. (1978), Wang and Crossman (1980), Wang (1984), Flaggs (1985), Dvorak and Laws (1986), Hahn et al. (1988), Nairn (1989), Boniface et al. (1991), Zang and Gudmundson (1993), Xia et al. (1993), Chatterjee et al. (1993) and Hashin (1996). The application of an energy criterion needs to be combined with a method of calculating the energy release at crack formation. Examples of such methods given in the above works include shear-lag analyses, approximate expressions for the crack opening displacements of matrix cracks and variational methods.

The other main approach for the description of matrix cracking is to adopt some type of stress or strain criterion. Such criteria are found in the works by Garrett and Bailey (1977a, b), Parvizi and Bailey (1978), Flaggs and Kural (1982), Peters (1984), Fukunaga et al. (1984), Altus and Ishai (1986, 1990), Jen and Sun (1990), Crocker et al. (1996) and Li and Wisnom (1996). Also when using this approach, the stresses and strains in the vicinity of the cracks need to be predicted in order to enable a description of the laminate behaviour during loading. The methods which are used for this purpose are basically the same as those used in combination with the fracture mechanics approach for crack evolution description. In addition to this, the methods using a critical stress to describe crack growth are often applied in combination with a statistical treatment of the ply strength distribution. A more detailed review of different methods for prediction of matrix crack evolution in composite laminates is found in the work by Nairn and Hu (1994).

In the present work, results from an experimental investigation concerning matrix cracking in extension and bending are presented. The experiments involve $(0^\circ/90^\circ_n)_S$ cross-ply laminates, $(0^\circ_n/90^\circ_n/+45^\circ_n/-45^\circ_n)_S$ quasi-isotropic laminates and $(0^\circ_n/+45^\circ_n/-45^\circ_n)_S$ laminates. An energy release rate criterion and a strain criterion for crack initiation and progression are applied and compared to experimental data. The ply stresses at the onset of cracking are also studied. The validity and applicability of the different criteria for the considered material are discussed. Based on the strain criterion, damage evolution is simulated and the resulting load–deformation relations are compared to the ones measured experimentally.

2. Theoretical basis

2.1. Two-dimensional laminate theory for laminates without cracks

The well-known two-dimensional laminate theory incorporating bending and extension will serve as a basis for the derivation of a damage dependent constitutive law. In the following, characters with superscript letters denote local ply properties and characters without superscripts denote global effective laminate properties. Matrix transpose is indicated by a superscript 'T'. Consider a general two-dimensional laminate consisting of N plies. Ply k is characterized by its position between the coordinates h^{k-1} and h^k in the laminate thickness direction. The ply thickness t^k is hence calculated as $t^k = h^k - h^{k-1}$, and the ply midplane is characterized by the coordinate z^k

defined as $z^k = (h^k + h^{k-1})/2$. The laminate midplane corresponds to $z = 0$. Introduce also the plane stress stiffness matrix $\boldsymbol{Q}^k$ and the vector of in-plane thermal expansion $\boldsymbol{\alpha}^k$ of ply k. The load and deformation of the laminate are presented as the familiar forces and moments per unit area, and as the in-plane strains and curvatures, respectively. Allowing also for thermal expansion, the load–deformation relation of the virgin laminate may by use of Kirchhoff laminate theory be written as

$$\begin{pmatrix} \boldsymbol{N} \\ \boldsymbol{M} \end{pmatrix} = \begin{pmatrix} \boldsymbol{C}_{\mathrm{EE}} & \boldsymbol{C}_{\mathrm{EB}} \\ \boldsymbol{C}_{\mathrm{BE}} & \boldsymbol{C}_{\mathrm{BB}} \end{pmatrix} \begin{pmatrix} \boldsymbol{\varepsilon} \\ \boldsymbol{\kappa} \end{pmatrix} + \begin{pmatrix} \boldsymbol{\delta}_{\mathrm{E}} \\ \boldsymbol{\delta}_{\mathrm{B}} \end{pmatrix} \Delta T, \tag{1}$$

where

$$\begin{aligned} \boldsymbol{C}_{\mathrm{EE}} &= \sum_{k=1}^{N} t^k \boldsymbol{Q}^k \\ \boldsymbol{C}_{\mathrm{EB}} &= \boldsymbol{C}_{\mathrm{BE}} = \sum_{k=1}^{N} t^k z^k \boldsymbol{Q}^k \\ \boldsymbol{C}_{\mathrm{BB}} &= \sum_{k=1}^{N} t^k \left[(z^k)^2 + \frac{(t^k)^2}{12} \right] \boldsymbol{Q}^k \end{aligned} \tag{2}$$

and

$$\begin{aligned} \boldsymbol{\delta}_{\mathrm{E}} &= -\sum_{k=1}^{N} t^k \boldsymbol{Q}^k \boldsymbol{\alpha}^k, \\ \boldsymbol{\delta}_{\mathrm{B}} &= -\sum_{k=1}^{N} t^k z^k \boldsymbol{Q}^k \boldsymbol{\alpha}^k. \end{aligned} \tag{3}$$

The laminate theory for the undamaged laminate is thus established in eqns (1)–(3). By introduction of the 6×1 vectors of generalized forces $\boldsymbol{P}$ and extensions $\boldsymbol{e}$ as

$$\boldsymbol{P} = \begin{pmatrix} \boldsymbol{N} \\ \boldsymbol{M} \end{pmatrix} \quad \boldsymbol{e} = \begin{pmatrix} \boldsymbol{\varepsilon} \\ \boldsymbol{\kappa} \end{pmatrix}, \tag{4}$$

the relation in eqn (1) may be written on a contracted form as

$$\boldsymbol{P} = \boldsymbol{C}\boldsymbol{e} + \boldsymbol{d}\Delta T, \tag{5}$$

where the 6×6 stiffness matrix $\boldsymbol{C}$ is composed of the 3×3 sub-matrices from eqn (1) and 6×1 vector $\boldsymbol{d}$ contains the thermal stress coefficients $\boldsymbol{\delta}_{\mathrm{E}}$ and $\boldsymbol{\delta}_{\mathrm{B}}$. The expression in eqn (1) may be inverted to achieve the generalized strains as functions of the applied load as

$$\begin{pmatrix} \boldsymbol{\varepsilon} \\ \boldsymbol{\kappa} \end{pmatrix} = \begin{pmatrix} \boldsymbol{S}_{\mathrm{EE}} & \boldsymbol{S}_{\mathrm{EB}} \\ \boldsymbol{S}_{\mathrm{BE}} & \boldsymbol{S}_{\mathrm{BB}} \end{pmatrix} \begin{pmatrix} \boldsymbol{N} \\ \boldsymbol{M} \end{pmatrix} + \begin{pmatrix} \boldsymbol{\alpha}_{\mathrm{E}} \\ \boldsymbol{\alpha}_{\mathrm{B}} \end{pmatrix} \Delta T, \tag{6}$$

or on a contracted form analogous to eqn (5) as

$$\boldsymbol{e} = \boldsymbol{S}\boldsymbol{P} + \boldsymbol{a}\Delta T. \tag{7}$$

Ply residual stresses which may be present in the laminate due to anisotropic thermal and chemical shrinkage during manufacturing do not contribute to the overall laminate forces and moments per unit length. The self equilibrium of the initial residual stresses has been exploited in the derivation of the laminate equations above.

2.2. The stress–strain relation of laminates containing matrix cracks

The laminate theory will now be extended to take into account also the effects of a certain number of matrix cracks. Consider a general two-dimensional laminate consisting of N laminae according to the previous subsection. A global coordinate system is defined by the axes X_1 and X_2 in the laminate plane and the axis X_3 pointing in the thickness direction. The axes Y_1^k, Y_2^k and Y_3^k define the local coordinate system in ply k. The fibres in ply k are aligned with the Y_1^k-axis, and the Y_2^k-axis defines the direction normal to the fibres but in the plane of the laminate. The axis Y_3^k is directed normal to the laminate plane, and is hence parallel to the X_3-axis. A state of damage in the form of transverse matrix cracks is assumed to prevail according to Fig. 1. In each ply, the cracks are presumed to be uniformly distributed and to be running in the local Y_1^k-direction. The crack state in ply k is determined from a crack density ρ^k defined as

$$\rho^k = \frac{t^k}{d^k}, \tag{8}$$

where d^k is the average distance between adjacent cracks.

In some situations, however, the matrix cracks do not grow to cover the entire width of the laminate, which may be the case in particular for off-axis plies. The average distance between

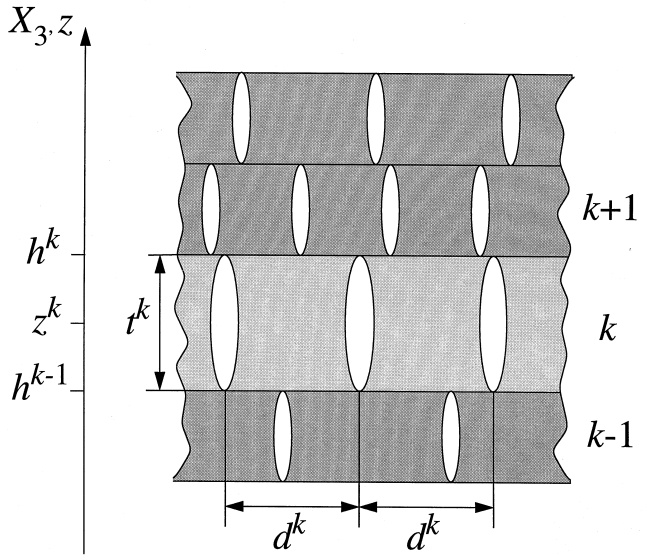

Fig. 1. A general two-dimensional laminate with a micro crack distribution. The damage state is determined by the crack densities $\rho^k = t^k/d^k$ in the separate plies.

adjacent cracks d^k may on such occasions be interpreted as a measure of the total sum of crack lengths per unit area in the ply under consideration. Using this definition, the crack density can be applied and calculated also for plies containing cracks that do not span the entire laminate width.

The presence of matrix cracks in one or several plies reduces the elastic energy of the loaded laminate. The strain energy $w_{(c)}$ per unit in-plane area of the damaged laminate may be written

$$w_{(c)} = \frac{1}{2}(\boldsymbol{e}-\boldsymbol{a}_{(c)}\Delta T-\boldsymbol{e}^{(R)})^T\boldsymbol{C}_{(c)}(\boldsymbol{e}-\boldsymbol{a}_{(c)}\Delta T-\boldsymbol{e}^{(R)})+\sum_{k=1}^{N} h^k(\Delta T,\boldsymbol{\sigma}^{k(R)}), \tag{9}$$

where $\boldsymbol{C}_{(c)}$, $\boldsymbol{a}_{(c)}$, and $\boldsymbol{e}^{(R)}$ are the stiffnesses, thermal expansion coefficients and residual stress induced eigenstrains, respectively, of the cracked laminate. Expressions for these crack density dependent quantities were derived in the work by Adolfsson and Gudmundson (1997), and are included in Appendix A for convenience. The effective properties presented by Adolfsson and Gudmundson (1997) are based on solutions for the stress intensity factors for problems closely related to that of matrix cracks in composite laminates. The calculated expressions for $\boldsymbol{C}_{(c)}$, $\boldsymbol{a}_{(c)}$, and $\boldsymbol{e}^{(R)}$ only contain ply property data and the crack densities ρ^k of the plies.

The energy which is stored in the laminate due to interlaminar constraints is contained in the functions $h^k(\Delta T,\boldsymbol{\sigma}^{k(R)})$, where the residual stress from manufacturing in ply k is denoted as $\boldsymbol{\sigma}^{k(R)}$. The functions h^k can be identified from expressions found in Adolfsson and Gudmundson (1997), which are contained in Appendix A. The vector of generalized forces $\boldsymbol{P}$ of the cracked laminate can now be derived by differentiation of the strain energy density $w_{(c)}$ in eqn (9) with respect to the vector $\boldsymbol{e}$ of generalized strains. The resulting expression is

$$\boldsymbol{P} = \boldsymbol{C}_{(c)}(\boldsymbol{e}-\boldsymbol{a}_{(c)}\Delta T-\boldsymbol{e}^{(R)}). \tag{10}$$

The resulting forces and moments per unit length for the cracked laminate are thus available as functions of the applied deformation and temperature. Explicit expressions for the components of the vector $\boldsymbol{P}$ for the cracked laminate from Adolfsson and Gudmundson (1997) are given in Appendix A. A simple model for matrix crack closure that was successfully used in the work by Adolfsson and Gudmundson (1994) may be applied to the expression in eqn (10). Matrix crack closure can be of importance especially for the behaviour of cracked composite laminates in bending.

2.3. Matrix crack initiation and progression

The constitutive relations from the previous section will now be combined with a matrix crack initiation and progression criterion. In this way equations for prediction of damage evolution in a composite laminate can be achieved. The damage evolution criterion may be formed on the basis of any scalar ply property considered relevant for controlling damage progression, such as energy release rate, stress or strain. The chosen property, denoted as Ψ^i in ply i, should be possible to calculate from the applied generalized strains $\boldsymbol{e}$, the change in temperature ΔT and the crack densities ρ^k.

The critical parameter for controlling damage evolution in the present work is assumed to depend only on the crack density in the current ply, and will be indicated $\Psi_c(\rho^i)$. This can be done without loss of generality in order to simplify the derivation. A damage dependent constitutive

law can now be constructed on an incremental form. The laminate is subjected to the global average generalized strain increments $\mathrm{d}\boldsymbol{e}$ and an incremental change in temperature $\mathrm{d}T$. The resulting change in crack density $\mathrm{d}\rho^i$ in ply i is then obtained from the conditions

$$\begin{aligned} &\mathrm{d}\rho^i = 0 \quad \text{if } \Psi^i < \Psi_{\mathrm{c}}(\rho^i) \quad \text{or if} \quad \Psi^i = \Psi_{\mathrm{c}}(\rho^i) \quad \text{and} \quad \mathrm{d}\Psi^i \leqslant 0 \\ &\mathrm{d}\Psi^i = \mathrm{d}\Psi_{\mathrm{c}} \quad \text{if} \quad \Psi^i = \Psi_{\mathrm{c}}(\rho^i) \quad \text{and} \quad \mathrm{d}\Psi^i > 0. \end{aligned} \tag{11}$$

Explicitly, the second expression in eqn (11), $\mathrm{d}\Psi^i = \mathrm{d}\Psi_{\mathrm{c}}$, yields a system of equations for the crack density changes $\mathrm{d}\rho^k$ as functions of the applied load increments $\mathrm{d}\boldsymbol{e}$ and $\mathrm{d}T$ according to the following:

$$\sum_{k=1}^{N} \frac{\partial \Psi^i}{\partial \rho^k}\mathrm{d}\rho^k + \frac{\partial \Psi^i}{\partial \boldsymbol{e}}\mathrm{d}\boldsymbol{e} + \frac{\partial \Psi^i}{\partial T}\mathrm{d}T = \frac{\mathrm{d}\Psi_{\mathrm{c}}}{\mathrm{d}\rho^i}\mathrm{d}\rho^i. \quad (i = 1, 2, \ldots, N, \text{ no sum over } i) \tag{12}$$

The resulting increment $\mathrm{d}\boldsymbol{P}$ in the global average load vector $\boldsymbol{P}$ as function of the applied deformation and temperature increments $\mathrm{d}\boldsymbol{e}$ and $\mathrm{d}T$ as well as of the crack density changes $\mathrm{d}\rho^k$ is then calculated as

$$\mathrm{d}\boldsymbol{P} = \frac{\partial \boldsymbol{P}}{\partial \boldsymbol{e}}\mathrm{d}\boldsymbol{e} + \frac{\partial \boldsymbol{P}}{\partial T}\mathrm{d}T + \sum_{i=1}^{N} \frac{\partial \boldsymbol{P}}{\partial \rho^i}\mathrm{d}\rho^i. \tag{13}$$

A damage dependent constitutive law is hence established by eqns (11)–(13). If instead the load increment $\mathrm{d}\boldsymbol{P}$ is prescribed, a system of non-linear equations for the generalized deformations $\mathrm{d}\boldsymbol{e}$ results.

By use of the expression for the strain energy of the damaged laminate in eqn (9), the energy release rate G^i for crack progression in ply i for a homogeneously strained laminate of in-plane area A can be calculated as

$$G^i = -\frac{\partial U}{\partial A^i} = -\frac{\partial (A w_{(\mathrm{c})})}{\partial A^i}, \tag{14}$$

where A^i is the crack surface area in ply i. The fact is utilized in eqn (14) that the potential energy U of the laminate equals the strain energy $W_{(\mathrm{c})} = A w_{(\mathrm{c})}$, since it is assumed that the deformations $\boldsymbol{e}$ are controlled. The area A^i can be related to the laminate in-plane area A and the crack density ρ^i through $A^i = \rho^i A$. From eqns (9) and (14), the energy release rate G^i is hence achieved as

$$\begin{aligned} G^i = &\left(\frac{\partial \boldsymbol{a}_{(\mathrm{c})}}{\partial \rho^i}\Delta T + \frac{\partial \boldsymbol{e}^{(\mathrm{R})}}{\partial \rho^i}\right)^{\mathrm{T}} \boldsymbol{C}_{(\mathrm{c})}(\boldsymbol{e} - \boldsymbol{a}_{(\mathrm{c})}\Delta T - \boldsymbol{e}^{(\mathrm{R})}) \\ &- \frac{1}{2}(\boldsymbol{e} - \boldsymbol{a}_{(\mathrm{c})}\Delta T - \boldsymbol{e}^{(\mathrm{R})})^{\mathrm{T}} \frac{\partial \boldsymbol{C}_{(\mathrm{c})}}{\partial \rho^i}(\boldsymbol{e} - \boldsymbol{a}_{(\mathrm{c})}\Delta T - \boldsymbol{e}^{(\mathrm{R})}) - \sum_{k=1}^{N} \frac{\partial h^k}{\partial \rho^i}. \end{aligned} \tag{15}$$

The energy release rate G^i in eqn (15) may now be used as the damage evolution controlling parameter Ψ^i according to eqns (11)–(13). A resistance curve may then be adopted for construction of matrix crack initiation and progression criteria. The resistance curve must be constructed on the basis of experimental results for the material under consideration.

The application of eqn (15) for prediction of matrix crack progression thus requires the derivatives of the effective thermoelastic laminate properties with respect to the ply crack densities. The derivatives of these properties are usually more difficult to calculate than the properties themselves. The finite element simulations given by Adolfsson and Gudmundson (1997) indicate, however, that also the derivatives of the effective properties are reasonably well described by the expressions seen in Appendix A.

3. Extensional and bending test procedures

3.1. Laminates and specimen preparation

The laminates used in the experiments were fabricated by Saab Military Aircraft in Linköping, Sweden, from commercially available prepregs. The glass/epoxy prepregs were Fibredux 913G-E-5-30%, which were heated at 4°C per minute to 125°C. The curing time was 60 min and the autoclave pressure was 0.6 MPa. The in-plane elastic properties of the material system were experimentally evaluated, and are presented in Table 1. The evaluation of the E-moduli and of the Poisson's ratio of the unidirectional ply was performed in accordance with standard ASTM D 3039/D 3039M-93, and the shear modulus was acquired by use of the procedure according to ASTM D 3518/D 3518M-91. The longitudinal and transverse thermal expansion coefficients which are used for calculation of residual stresses from manufacturing have been chosen as typical values for the present composite system, and were not experimentally determined in the present work.

Specimens with eight different lay-ups were tested in order to investigate effects of different fibre directions and different interlaminar constraints on the damage evolution. The lay-up configurations tested in extension were $(0^\circ/90^\circ_n/0^\circ)$ $(n = 1, 2, 4, 8)$ cross-ply laminates, $(0^\circ_n/90^\circ_n/+45^\circ_n/-45^\circ_n)_S$ $(n = 1, 2)$ quasi-isotropic laminates and $(0^\circ_n/+45^\circ_n/-45^\circ_n)_S$ $(n = 1, 2)$ laminates. In the bending experiments, two laminate types were tested, $(90^\circ_2/0^\circ_2/-45^\circ_2/+45^\circ_2)_S$ and $(90^\circ_2/-45^\circ_2/+45^\circ_2)_S$.

The specimen geometry was basically chosen according to the ASTM D 3039/D 3039M-93 standard. The width of the test samples was thus approximately 25.0 mm and the specimen length was around 250 mm. Since, in the present investigation, edge replication technique is used to monitor the damage state, a thorough preparation of the specimen edges is necessary. The edges were wet sanded in a total of nine stages of abrasive machining comprising a range of FEPA

Table 1
The characteristic engineering constants and thicknesses of the unidirectional glass fibre reinforced epoxy (GFRP) ply. The elastic properties were experimentally evaluated while the thermal expansion coefficients were chosen as typical values for the considered material system

Type	E_L (GPa)	E_T (GPa)	ν_{TL}	G_{LT} (GPa)	α_L (μK^{-1})	α_T (μK^{-1})	Ply thickness (mm)	Density (kg/m^3)
GFRP	46	18	0.29	7.9	6.72	29.3	0.125	1930

gradings from P100 to P1200. At all stages, an oil-carrier was used to prevent clogging of the abrasive cloth.

3.2. Testing procedure

Tests were conducted in quasi-static extension and in bending. The tension tests were performed using an MTS 981.93 servo-hydraulic device with an MTS 312.21 SP loadframe, an MTS 204.63 actuator and an MTS 661.21B-03 load cell. Test control was enabled using an INSTRON 8500 PLUS controlling unit. The specimens were clamped between MTS hydraulic wedge grips. In order to avoid sliding, P150 grit sanding paper was attached to the specimens before insertion in the grips. Test data were recorded on a personal computer via a Scorpio Data Logger SI 3535F from Solartron Instruments. The load, the grip displacement and four transverse strains were recorded. The strains were measured using Showa foil strain gauges. Two transverse strains on each side of the specimen were monitored in order to avoid interference from bending effects. The final value for the transverse strain was taken as the average of the four recorded strains. The longitudinal strains were calculated form the grip displacements taking the compliance of the testing machine into account.

The tension specimens were tested at a cross-head speed of 0.025 mm per s. An initial unloading was performed early in the loading process to capture the elastic properties of the virgin laminate. At certain stages of the following process, unloadings were carried out to monitor the changes in the elastic properties as a function of the laminate damage. The damage state in terms of matrix cracks was investigated by means of edge replication. Tape of clean cellulose acetate plastic was attached to the specimen edge, then softened with acetone. The cellulose tape was then gently pressed against the specimen edge until the tape had hardened enough for its removal. The replica could then be mounted on a microscope slide for convenient subsequent handling, microscope viewing and storage.

The state of cracking is thus recorded from studies of the specimen edges, where complicated three-dimensional effects generally prevail. The mere use of relatively narrow standard laminate specimens could imply that what is actually measured during the experiments are the tendencies to edge initiation of cracks. The three-dimensional edge effects could in particular complicate the comparisons between cross-ply laminates and laminates of more complicated lay-ups including off-axis plies. The use of a standard specimen size, however, enables comparisons with the results from previously performed investigations.

For the bending tests, an MTS 903.25 testing machine equipped with an MTS 305.03 load frame, an MTS 205.02 actuator and an HBM type U1 50 kg load cell was utilized. In order to obtain a constant and pure bending moment over the entire length of the bending specimen, a loading device according to Appendix B was constructed, using the servo-hydraulic actuator as a load source. A schematic of the device is shown in Fig. B1. An Orion 3530 Data Logging System from Solartron Instruments was used to collect the test data which consisted of the load, the grip displacement, two longitudinal strains and two transverse strains. The strains were measured using Showa foil strain gauges. Two strain gauges were mounted on each side of the bending specimens. The curvature of the specimens was calculated from the difference between the longitudinal strains on the two sides of the laminate divided by the laminate thickness. From the grip displacements of the testing machine, the angles of rotation at the ends of the bending specimen could be

calculated from purely geometrical considerations, which are accounted for in Appendix B. The angles of rotation are needed in order to calculate the applied bending moment from the information of the applied load available from the load cell. Unloadings were performed at certain load levels to capture the reduction in bending stiffness and transverse curvature as function of the progressing damage. The number of matrix cracks that occurred in the laminates was investigated by means of visual inspection using the naked eye.

4. Degraded elastic properties

4.1. Degraded elastic properties in extension

The reduced extensional E-moduli of the tested glass/epoxy cross-ply laminates are shown in Fig. 2. Three specimens of each of the four lay-ups were tested. The experimental data are indicated by filled symbols, and the results from the approximate analytic method presented in the work by Adolfsson and Gudmundson (1997) are represented by the solid lines. The corresponding in-plane Poisson's ratios for the considered laminates are shown in Fig. 3. The agreement between the analytic predictions and the experimental results is as can be seen acceptable for both the E-moduli and for the Poisson's ratios.

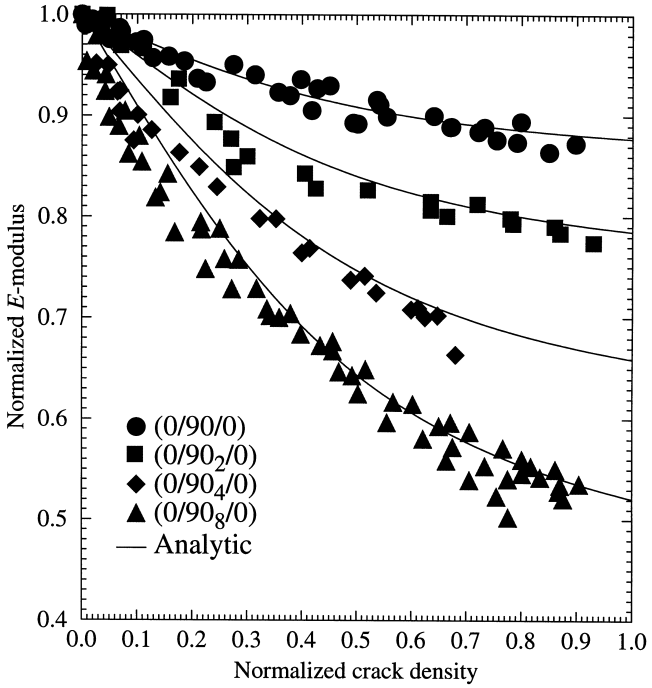

Fig. 2. The reduced longitudinal E-moduli for the glass/epoxy cross-ply laminates with matrix cracks. The experimental results are indicated by symbols and the analytic results are represented by solid lines.

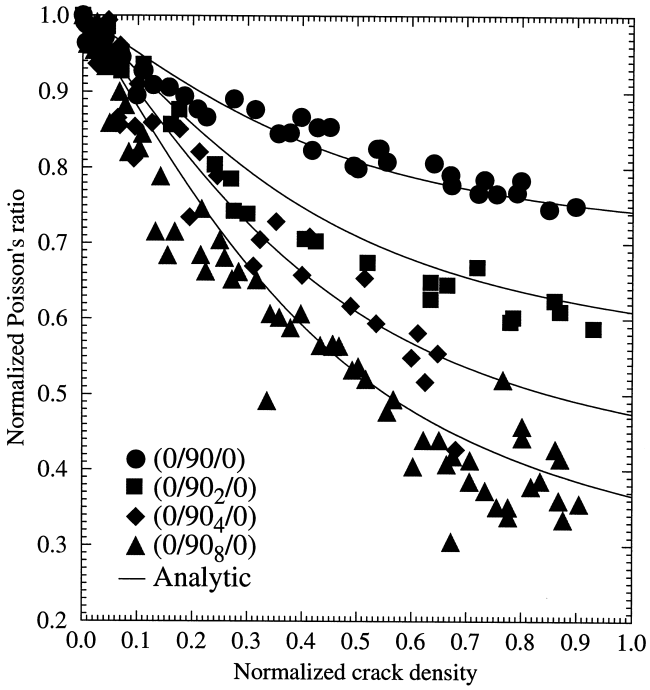

Fig. 3. The reduced in-plane Poisson's ratios for the glass/epoxy cross-ply laminates with matrix cracks. The experimental results are indicated by symbols and the analytic results are represented by solid lines.

It can be seen in Fig. 2 that for low crack densities, the experimentally measured stiffnesses are somewhat lower than the corresponding analytically calculated quantities. This would imply that the actual crack densities are higher than the measured ones. Since the crack densities were measured by use of an edge replication technique, one explanation to the discrepancies could be that cracks which are not detectable at the specimen edges exist in the laminates. Other experimental observations (Prosser et al., 1995; Lafarie-Frenot and Hénaff-Gardin 1991) suggest, however, that the cracks initiate at the specimen edges, why interior cracks seem less likely. For the thicker cross-ply laminates, that is $(0^\circ/90_2^\circ)_S$ and $(0^\circ/90_4^\circ)_S$, the matrix cracks were easily countable from visual inspection using the naked eye. In this inspection, the whole width of the laminate could be covered. There was a one to one correlation between the edge replication results and the results from visual inspection for those laminates. One could also be led to believe that other damage modes than matrix cracking play an active part in the degradation process, such as delamination and fibre fracture. No such additional damage could be detected in the examination of the edge replicas, though. An example of a replica from a $(0^\circ/90^\circ)_S$ laminate is shown in Fig. 4. It is seen that the cracks are evenly distributed and that the crack density is of the order of one.

From Fig. 3, it can be concluded that the relative reductions in the Poisson's ratios due to matrix cracking are larger than those in the E-moduli for the laminates under consideration. The trend is also clear that the scatter in the experimentally measured Poisson's ratio is larger than that in the

E-moduli. This might be explained by the fact that the transverse strains which form the basis for the calculation of the Poisson's ratios are evaluated using the signals from four foil strain gauges. The transverse strain is hence averaged over a distance of approximately 10 mm, compared to the longitudinal strain which is averaged over the full length of the specimen. The local effects of the damage evolution in the area of the strain gauges will then obviously have a strong influence on the measured transverse strains and thus equally affect the calculated Poisson's ratios.

The reduced *E*-moduli of the quasi-isotropic $(0_n^\circ/90_n^\circ/+45_n^\circ/-45_n^\circ)_S$ $(n = 1, 2)$ laminates are shown in Fig. 5. Two specimens of each of the two stacking sequences were tested. The experimental results are indicated by filled symbols and the corresponding analytically calculated *E*-moduli are shown by use of hollow symbols. The reason why there is a scatter in the analytic values is that there are cracks not only in the 90° plies but also in the $+45^\circ$ and -45° plies. The scatter in the analytic values hence only reflects the scatter in the experimentally measured crack densities. It is clear that the experimental values are in general lower than the theoretical ones. The major reason for this is that additional damage in the form of delaminations is present in the current laminates. Delaminations are clearly seen in Fig. 6, where a photograph of a replica from a $(0^\circ/90^\circ/+45^\circ/-45^\circ)_S$ laminate is shown.

There is a trend that the experimentally measured stiffness of the thinner $(0^\circ/90^\circ/+45^\circ/-45^\circ)_S$ laminates tend to be lower than those of the thicker $(0_2^\circ/90_2^\circ/+45_2^\circ/-45_2^\circ)_S$ laminates. This effect is also visible in the corresponding analytic results, but is considerably smaller in the latter case. This could imply that the actual crack densities are higher than those which are obtained from the edge replicas. The reason why this effect is more pronounced in the thinner laminates would in that case be that the crack opening displacements are proportional to the ply thickness. The cracks are thus more difficult to detect in a thinner laminate. The phenomenon could also be connected with the delaminations that occur in the laminate types under consideration, an example of which is shown in Fig. 6. The delamination area could not be detected from use of the edge replication technique. The only delaminations which were possible to detect were the delaminations at the specimen edges. A thorough presentation of the degree of delamination consequently cannot be presented herein. A first estimate of the degree of delamination could however be obtained from the edge replicas. The microscope examination of the replicas revealed that the number of visible delaminations was of the same order of magnitude for the thinner and the thicker laminates. The relative density of delaminations is then considerably higher in the thinner laminates, which could account for part of the observed difference in stiffness between the thinner and the thicker quasi-isotropic laminates. For the quasi-isotropic laminates, the reduction in Poisson's ratios were very small for all specimens tested.

The results of the experiments on the $(0_n^\circ/+45_n^\circ/-45_n^\circ)_S$ $(n = 1, 2)$ laminates are shown in Fig. 7. In this figure, like in Fig. 5, the scatter in the analytic data is not very large, and the difference between the thinner and the thicker laminates is negligible. The analytically calculated stiffness reduction, which should reflect the stiffness reduction due to the matrix cracks, is practically a linear function of the crack density indicated on the horizontal axis. This was also the case in Fig. 5, but this phenomenon must be considered a mere coincidence attributed to the relation between the crack densities of the different plies of the laminates. The scatter of the experimental data in Fig. 7 is fairly large. The analytic results in this case, as opposed to in Fig. 5, form an approximate average of the experimental data. Due to very small relative reductions, results concerning the Poisson's ratios of the current laminates will not be presented.

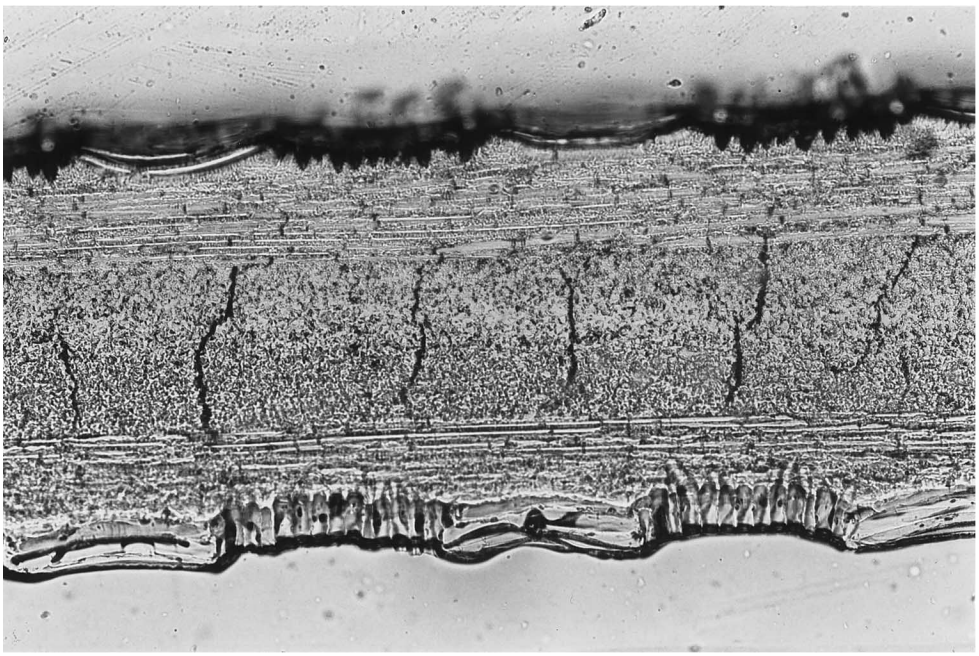

Fig. 4. A typical damage pattern of a cross-ply laminate. The illustration shows a $(0^\circ/90^\circ_2/0^\circ)$ laminate subjected to a strain of two per cent. The resulting matrix crack density is around unity.

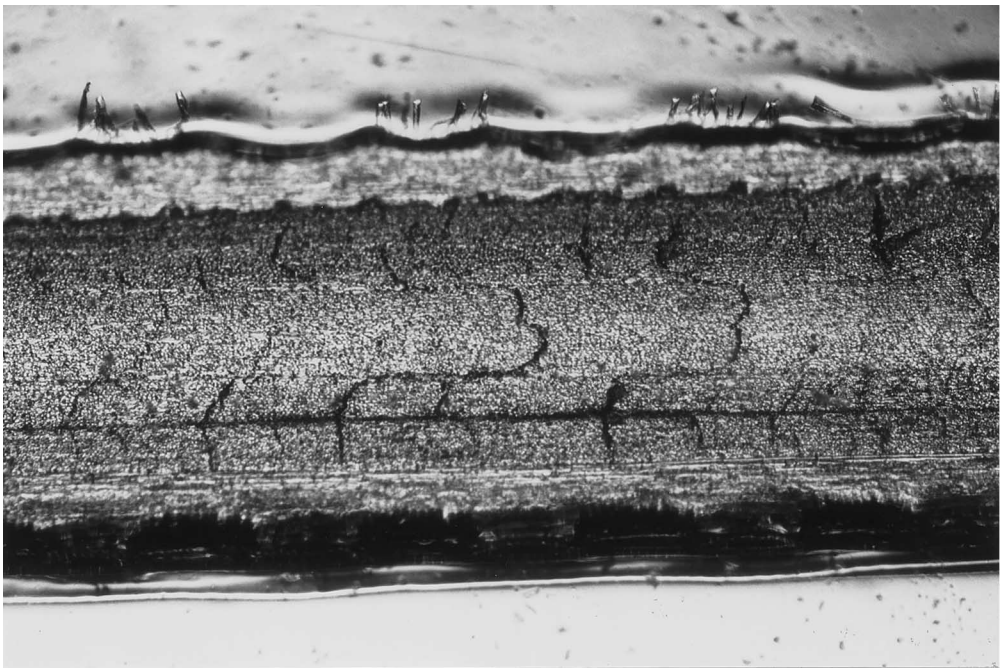

Fig. 6. A damage pattern of a $(0^\circ/90^\circ/+45^\circ/-45^\circ)_S$ subjected to a strain of two and a half per cent. A long delamination between the lower 90° and $+45^\circ$ plies is visible in the lower part of the photograph. It is also seen that cracks in the 90° plies promote the forming of cracks in the adjacent $+45^\circ$ plies at the specimen edges. The cracks in the $+45^\circ$ plies are connected to the cracks in the centre -45° ply via delaminations.

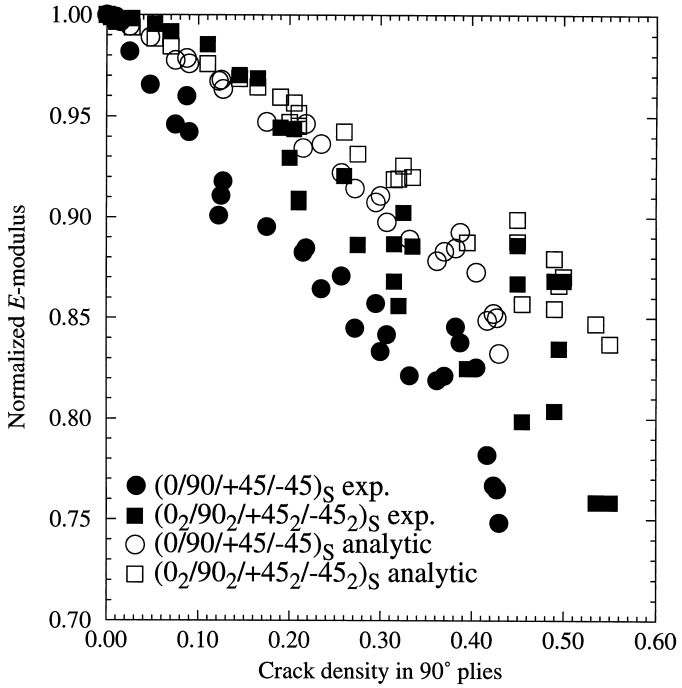

Fig. 5. The reduced E-moduli for the $(0_n^\circ/90_n^\circ/+45_n^\circ/-45_n^\circ)_S$ ($n = 1, 2$) laminates. The experimental results are indicated by the filled symbols. The hollow symbols represent the analytic results for the corresponding properties based on the experimentally measured crack densities.

4.2. Reduced stiffnesses in bending

The reduced flexural moduli for the bending specimens are shown in Figs 8 and 9 $(90_2^\circ/0_2^\circ/-45_2^\circ/+45_2^\circ)_S$ laminates and the $(90_2^\circ/-45_2^\circ/+45_2^\circ)_S$ laminates, respectively. It is seen that there is a considerable scatter in the experimentally evaluated flexural moduli. The scatter may relate to deficiencies in the experimental equipment. The bending device according to Appendix B was used in a horizontal position on a teflon plastic plate prepared with silicone spray to reduce its frictional effect. The frictional forces might in any case have influenced the measured relation between curvature and applied bending moment. It can also have been the case that the wires used in the experimental set-up were too stiff in bending, which would also have disturbed the achieved results. The specimens which were tested in bending were bent two times each, so that cracking occurred in tension in the 90° plies on both sides of the laminates. In such a case, it is possible to investigate the effect of matrix crack closure, which should be present on the side of the specimen which exhibits compressive stresses. No non-linearities that could be said to originate from matrix crack closure could be seen, however. It was not possible to see a clear difference between the laminates that contained cracks on only one side and the laminates that contained cracks on both sides, which is evident from Figs 8 and 9. This could be interpreted as if the cracks which experience compression close very early in the loading process. It could also be an effect of an insufficient resolution in the stiffness measurements. Although the scatter in the data is high, this last expla-

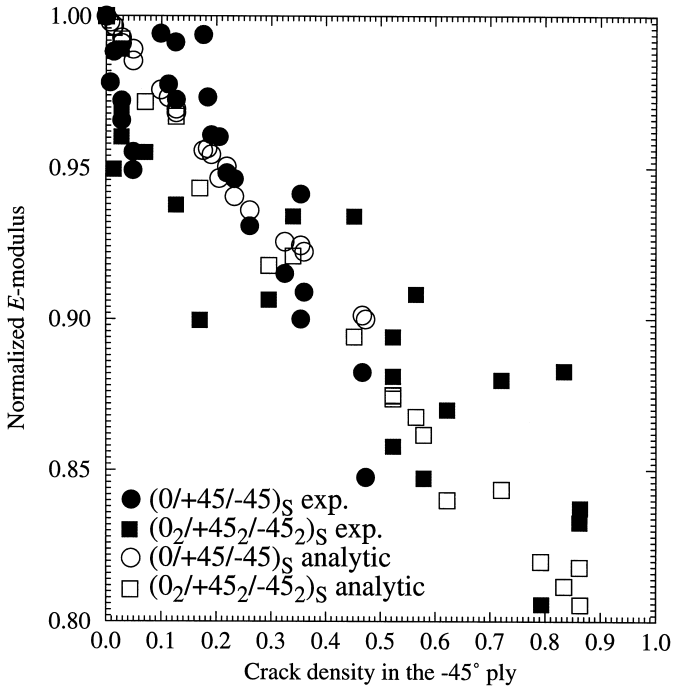

Fig. 7. The reduced E-moduli for the $(0_n^\circ/+45_n^\circ/-45_n^\circ)_S$ $(n = 1, 2)$ laminates. The experimental results are indicated by the filled symbols. The hollow symbols represent the analytic results for the corresponding properties based on the experimentally measured crack densities.

nation seems less likely. The trend is clear that the bending stiffness decreases with an increasing crack density, and open cracks on both sides of the laminate would give twice as high stiffness reductions compared to the case when only the cracks on one side of the laminates are opened. The reductions in the presented E-moduli are fairly small, which also increases the relative importance of the experimental scatter.

5. Damage evolution

The more difficult problem of the construction of a damage dependent constitutive law is usually that of predicting damage initiation and progression. In the present investigation, two different approaches are chosen in an attempt to characterize the damage initiation and progression. All ply stresses and strains reported herein have been corrected for thermal residual stresses from manufacturing. A decrease in temperature of 100°C has been assumed, and the thermal expansion coefficients presented in Table 1 have been used to calculate the resulting residual stresses and corresponding residual strains.

5.1. Matrix crack initiation

Matrix crack initiation criteria are often based on a critical strain or on a critical stress. Fracture mechanics approaches for the prediction of the onset of cracking seem somewhat problematic,

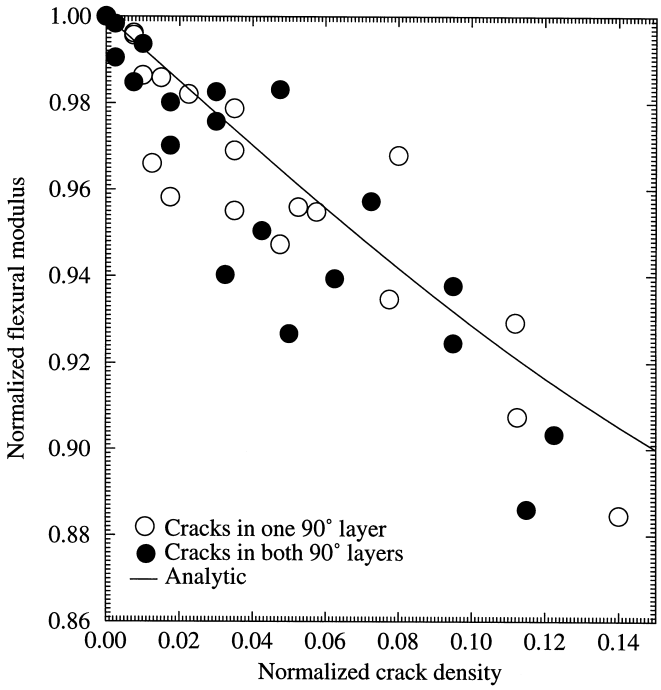

Fig. 8. The reduced equivalent flexural E-moduli for the $(90_2^\circ/0_2^\circ/-45_2^\circ/+45_2^\circ)_S$ laminates tested in bending. Cracks appear only in the 90° plies. The corresponding analytic results are indicated by solid lines. The hollow symbols indicate the results where there are cracks on only one side of the specimens. The filled symbols represent the stiffnesses of the specimens when containing cracks in the 90° on both sides, that is after having been bent twice.

unless based on the flaws which may be assumed to exist in the material prior to matrix cracking. Otherwise, there are no cracks to determine the initial fracture mechanics parameters from. The expression for the energy release rate which has been derived in the present work reduces to a critical stress criterion with a correction for the ply thickness for vanishing crack densities. As can be seen in Fig. 10, the energy release rates at the onset of cracking calculated from eqn (15) for the cross-ply laminates differ considerably from one laminate thickness to another. The energy release rates were explicitly evaluated using the expression for the strain energy density found in eqn (A8) inserted into eqn (14). The corresponding ply strains are shown in Fig. 11, still exclusively for the cross-ply laminates. The scatter in the strains when cracks appear for the different laminates is lower than that of the corresponding energy release rate values. In order to get a more complete picture of the crack initiation characteristics for the different laminates investigated in bending as well as in extension, the in-plane normal and shear stresses and strain on the weak planes in the plies at the onset of cracking have been calculated. On the basis of these calculations, the results from different ply angles and different ply stacking sequences are compared.

The normal strains and the shear strains at damage initiation are shown in Fig. 12. The corresponding normal stresses and shear stresses have been calculated using ordinary laminate theory for an uncracked laminate, and can be seen in Fig. 13. The crack initiation locus which is implied by these two figures suggests that the main damage initiation mechanism is of mode I type,

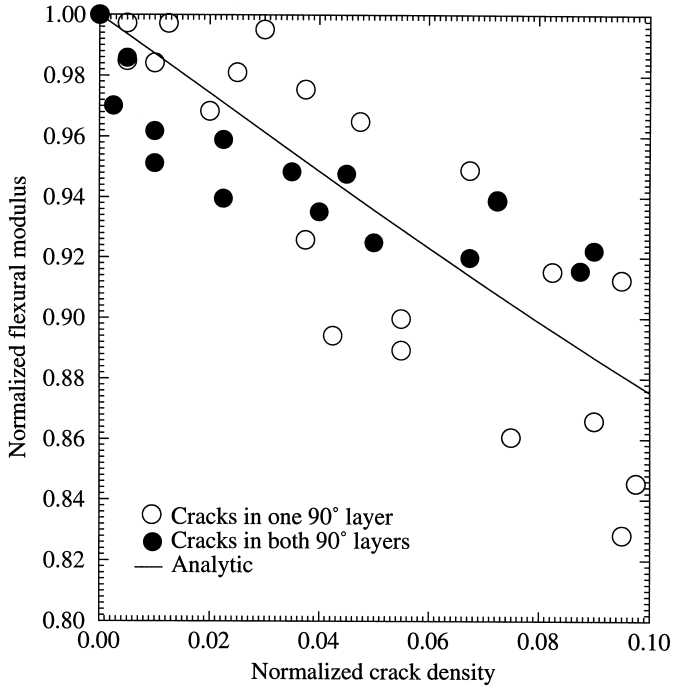

Fig. 9. The reduced equivalent flexural E-moduli for the $(90_2^\circ/-45_2^\circ/+45_2^\circ)_S$ laminates tested in bending. Cracks appear only in the 90° plies. The corresponding analytic results are indicated by solid lines. The hollow symbols indicate the results where there are cracks on only one side of the specimens. The filled symbols represent the stiffnesses of the specimens when containing cracks in the 90° on both sides, that is after having been bent twice.

since there is only a small decrease in the normal stresses needed for the onset of cracking for the cases where considerable shear stresses are present.

5.2. Matrix crack progression in extension

Two different ways of characterizing the matrix crack evolution will be chosen in the present investigation. The energy release rates defined in eqn (15) are calculated from the experimentally measured applied load and resulting crack densities. The global strains transverse to the fibres in the different plies are also calculated and related to the degree of cracking in the ply under consideration.

The energy release rates for the cross ply laminates are shown in Fig. 10 related to the crack densities in the 90° plies. As can be seen, there is a strong dependency on the thickness of the 90° plies in the calculated energy release rates. The general trend reported on in other experimental investigations (see e.g. Garrett and Bailey, 1977a) is that matrix cracking occurs for lower stresses in thick plies than in thinner plies. Since the expression for the energy release rate in eqn (15) accommodates a linear dependence on the ply thickness, it might be expected that it could render an acceptably accurate description of the matrix crack progression.

In the literature, the energy release rate concept for prediction of matrix crack evolution has

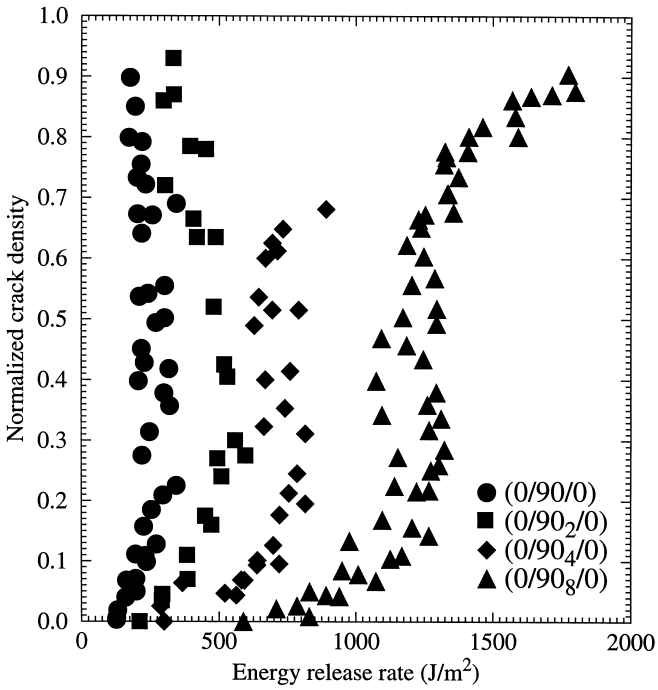

Fig. 10. The crack densities as functions of the energy release rate calculated according to eqn (15) for the tested cross-ply laminates. The energy release rates were calculated taking residual stresses from manufacturing into account.

proven successful for small ply thicknesses. For thicknesses larger than some transition thickness, the fracture mechanics approach fails since it predicts an ever decreasing strength with increasing thickness. In order to cope with this problem, Wang and Crossman (1980) introduced the concept of initial flaw size. The idea is that the cracking process depend on the size of initial flaws in the material. For ply thicknesses much larger than the flaw size, the crack initiation is independent of ply thickness. If, on the other hand, the flaw size is of the order of ply thickness or larger, then the ply thickness sets a limit for the flaw size, and the ply thickness will influence the ply strength. These ideas are supported by the results of Parvizi et al. (1978), which show that the ply cracking strain is independent of the ply thickness provided that the ply thickness is large enough. Similar tendencies can be traced in the works by Flaggs and Kural (1982) and by Harrison and Bader (1983). Results with the same implication were also obtained by Hahn et al. (1988), who, when using an energy release rate resistance curve for matrix cracking, saw a marked ply thickness dependence.

As can be seen in Fig. 11, for the material under consideration, there is a rather weak dependence on the ply thickness in the curve relating crack density to longitudinal strain. This could indicate that the initial flaw size for the material under consideration is smaller than the smallest ply thickness used in the experiments. For use in further comparisons and simulations, a quadratic curve was fitted to the data presented in Fig. 11, resulting in the following expression for the crack density as a function of the applied strain transverse to the fibres:

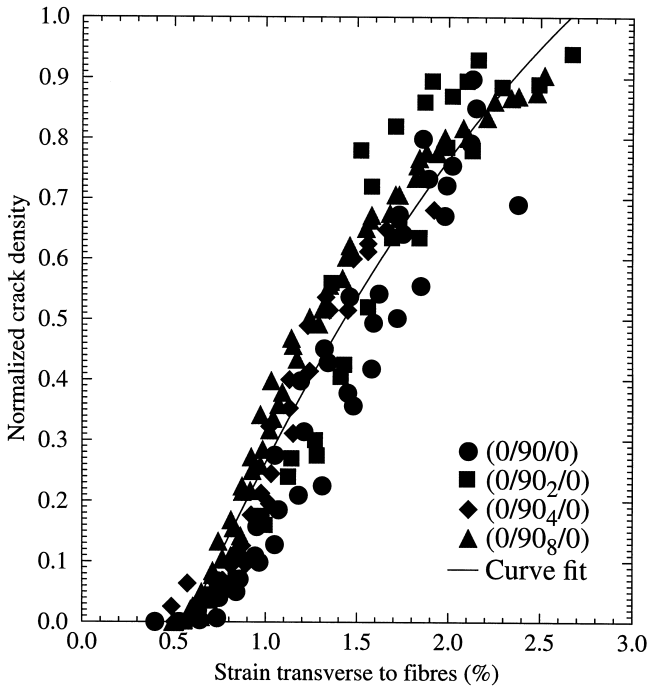

Fig. 11. The crack densities as functions of the applied strains for the tested cross-ply laminates. Thermal residual strains from manufacturing were incorporated.

$$\rho = 0 \quad \varepsilon < 5.9 \times 10^{-3}$$

$$\rho = -0.42 \times 76\varepsilon - 870\varepsilon^2 \quad 5.9 \times 10^{-3} \leqslant \varepsilon \leqslant 3.0 \times 10^{-2}. \tag{16}$$

The fitted expression presented in eqn (16) is intended merely to serve as an example of a resistance curve in order to enable subsequent damage evolution simulations for the material under consideration in the indicated strain interval. It is seen in Fig. 11 that the present glass/epoxy material can sustain considerable strains before failure. It can also be noticed that the crack densities do not exceed unity for any of the considered cross-ply laminates. Considering the energy release rates in Fig. 10, it is clear that the thickness of the plies have too large an influence on the calculated energy release rates compared to a case where the energy release rate actually characterizes the damage evolution. If the parts of the curves in Fig. 10 are considered where the energy release rates are almost constant, the values for the different ply thicknesses relate to each other approximately as 1.0 : 2.0 : 3.1 : 5.3 for the $(0^\circ/90^\circ_n/0^\circ)$ $(n = 1, 2, 3, 4)$ laminates. If these values are normalized by division by the number of 90° plies in each laminate type, the ratios change to 1.0 : 1.0 : 0.78 : 0.66. From Fig. 11, it can be noticed that the crack densities are somewhat lower for the thinner laminates than for the thicker for a certain applied strain. The differences are however small. The scatter in the experimental data is also larger for the thinner plies, since for these only edge replication technique was used to monitor the damage. The edge replicas only

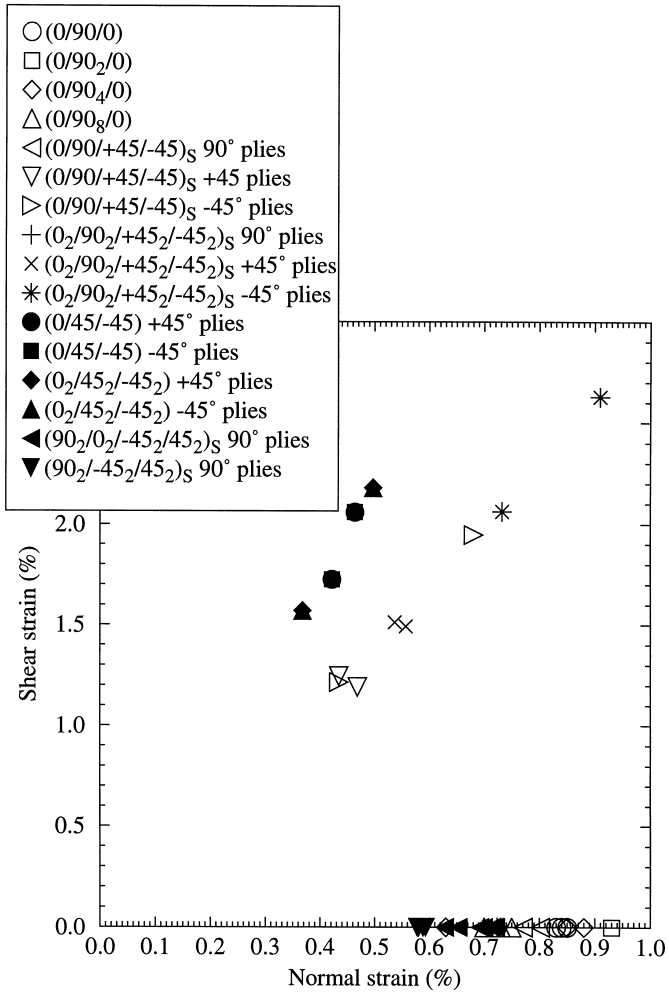

Fig. 12. The normal and shear ply strains transverse to the fibres including residual strains at the onset of cracking for the laminates tested in extension and the laminates tested in bending.

enable an averaging of the crack density over a length of 50 mm, while for the thicker laminates the full length of the testing specimens were visually inspected for matrix cracks.

The constitutive equation incorporating damage evolution presented in eqns (11)–(13) may now be used to simulate the stress–strain behaviour of the tested cross-ply laminates. The fitted expression in eqn (16) is adopted as a resistance curve for matrix crack initiation and progression. The results of these simulations are shown in Fig. 14. Since the utilized resistance curve was originally fitted to the experimental damage evolution data of the cross-ply laminates, it is not surprising that the agreement is fairly good between the simulations and the experiments. The load was applied using controlled deformations requiring vanishing global stress transverse to the loading direction, thus involving a combination of prescribed stresses and strains, which calls for

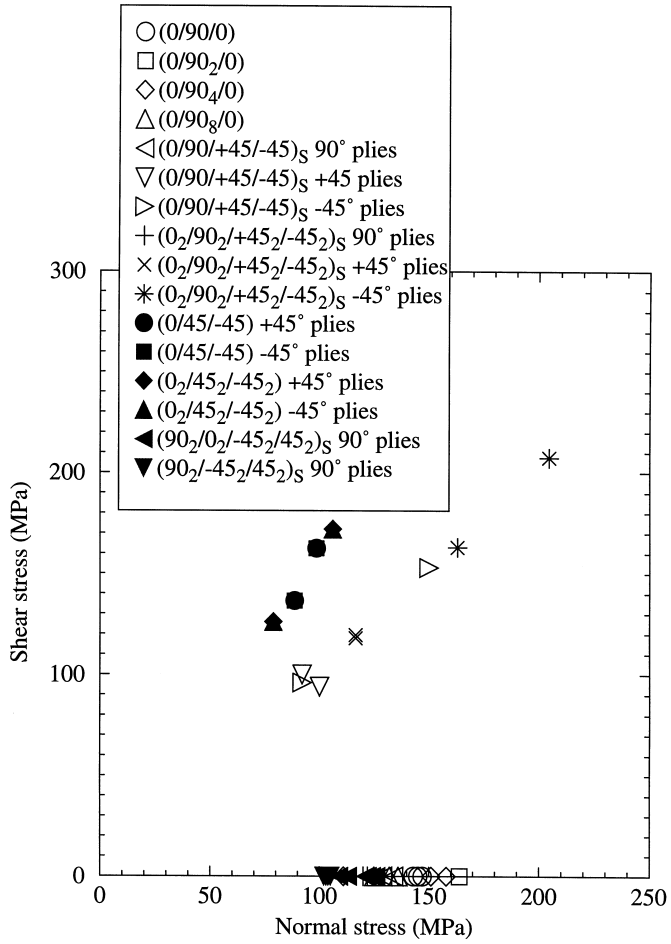

Fig. 13. The normal and shear ply stresses transverse to the fibres including residual stresses at the onset of cracking for the laminates tested in extension and the laminates tested in bending.

the solution of a system of equations in each increment. Since the possibility of having crack closure was taken into consideration in all simulations, the system becomes non-linear. The simulations were performed using 1000 increments in order to enable fast convergence in each increment.

It can be seen in Fig. 14 that the slope of the stress–strain curve increases slightly after the first cracks were initiated. This may seem surprising considering that the crack density is still increasing, and hence continuously reduces the global E-modulus of the laminate. The tangent E-modulus of the material, however, depend also on the rate of increase in crack density. Since the crack density increases rapidly with the applied strain in the beginning of the process, but more slowly towards the end of an experiment, the tangent E-modulus increases. The size of the tangent E-modulus is thus the result of a competition between the reduction in stiffness and the reduction in crack growth rate.

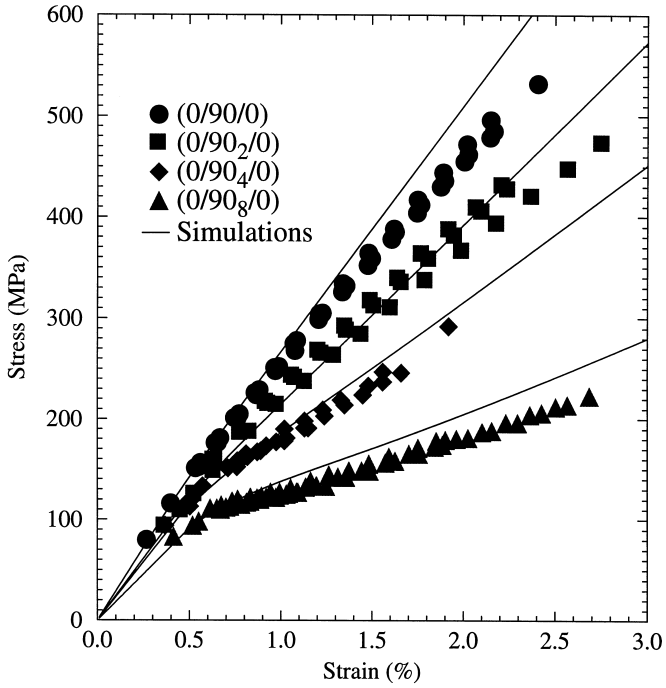

Fig. 14. The stress–strain behaviour of the tested cross-ply laminates. The experimental results are indicated by the symbols and the simulations performed by use of eqns (11)–(13) and (16) are represented by solid lines.

Other investigations support the observations that the critical strain for formation of matrix cracks has a weak dependence on the ply thickness, provided that the ply thickness exceeds some typical value. Such observations have been made by, among others, Parvizi et al. (1978) and Bailey et al. (1979). This typical value has been suggested to be related to the initial flaw size according to the discussion in the previous section.

The results of the testing of the quasi-isotropic $(0^\circ_n/90^\circ_n/+45^\circ_n/-45^\circ_n)_S$ $(n = 1, 2)$ laminates are shown in Fig. 15. The crack density in each of the plies is related to the strain transverse to the fibres in that specific ply. The solid line is the curve fit obtained from the cross-ply laminates according to eqn (16). There is no significant difference between the thicker and the thinner plies concerning matrix crack evolution. For the thicker laminate, the crack densities of the 90° plies tend to be higher than those of the thinner laminates. Comparing the results for 90° plies in Fig. 15 with the corresponding crack densities for the cross-ply laminates in Fig. 11, it is revealed that for the same strain, the crack densities are considerably lower in the quasi-isotropic laminates. This could be a result of the fact that in the quasi-isotropic laminates, as opposed to in the cross-ply laminates, delaminations play an active part in the damage process for the higher strain levels under consideration. Stresses at the ply interfaces are then released by the formation of delaminations instead of by matrix crack progression. A long delamination is seen between the lower 90° and $+45^\circ$ plies in a $(0^\circ/90^\circ/+45^\circ/-45^\circ)_S$ laminate in Fig. 6. The three-dimensional effects that are active at the specimen edges may also account for the differences between the cross-ply laminates and the more complicated laminates.

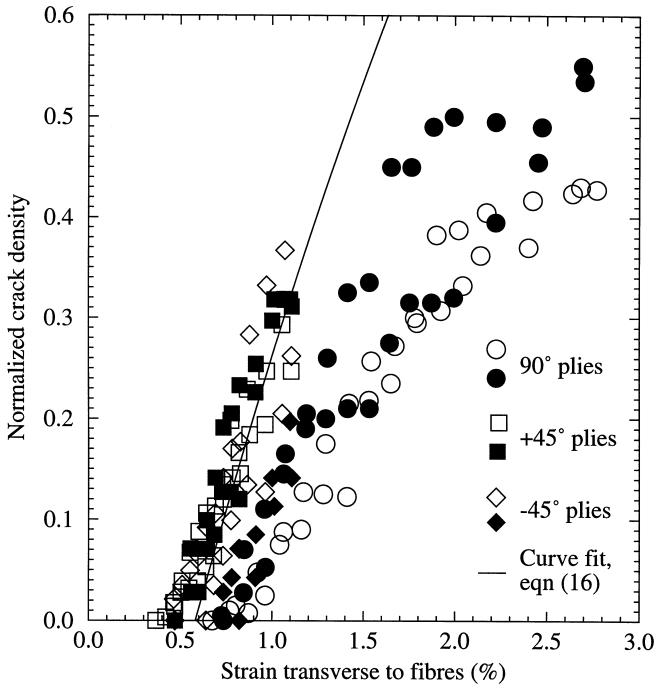

Fig. 15. Crack densities as functions of the applied strains transverse to the fibres in the separate plies for the $(0_n^\circ/90_n^\circ/+45_n^\circ/-45_n^\circ)_S$ $(n=1,2)$ laminates. The hollow symbols indicate the experimental results for the $(0^\circ/90^\circ/+45^\circ/-45^\circ)_S$ and the filled symbols represent the experimentally measured crack densities of the $(0_2^\circ/90_2^\circ/+45_2^\circ/-45_2^\circ)_S$ laminates. The solid line indicates the corresponding crack evolution for the cross-ply laminates according to Fig. 11 and eqn (16).

In Fig. 16, the crack densities of the $+45^\circ$ and -45° plies of the $(0_n^\circ/+45_n^\circ/-45_n^\circ)_S$ $(n=1,2)$ laminates are depicted. There is a major difference between the crack progression characteristics of the present figure and that of the quasi-isotropic laminates in Fig. 15. The matrix crack evolution of the off-axis plies in the $(0_n^\circ/+45_n^\circ/-45_n^\circ)_S$ laminates is considerably faster than in the cross-ply laminates. This is so in particular for the thicker plies. This phenomenon is somewhat surprising considering the effects of coupling between the matrix cracks of adjacent plies. In the quasi-isotropic laminates, cracks appear first in the 90° plies, which also promotes the forming of matrix cracks in the neighbouring $+45^\circ$ plies. The appearance of cracks in the $+45^\circ$ plies in turn facilitates the initiation and progression of cracks in the centre -45° plies due to the stress concentrations at the matrix crack tips. This coupling effect is visualized in Fig. 6, where it is seen that the cracks of the different plies tend to meet at the crack tips on the edges of the specimens. In some cases, the crack tips connect via a delamination. With this in mind, it could be expected that cracking would commence earlier in the off-axis plies of the quasi-isotropic laminates. In the $(0_n^\circ/+45_n^\circ/-45_n^\circ)_S$ $(n=1,2)$ laminates, the number of cracks per mm in the $+45^\circ$ and the -45° plies are not very different. The normalized crack density presented in the diagram, however, will be considerably larger for the -45° layer due to its larger thickness.

A simulation of the load as function of the applied strain for the $(0_n^\circ/90_n^\circ/+45_n^\circ/-45_n^\circ)_S$ laminates

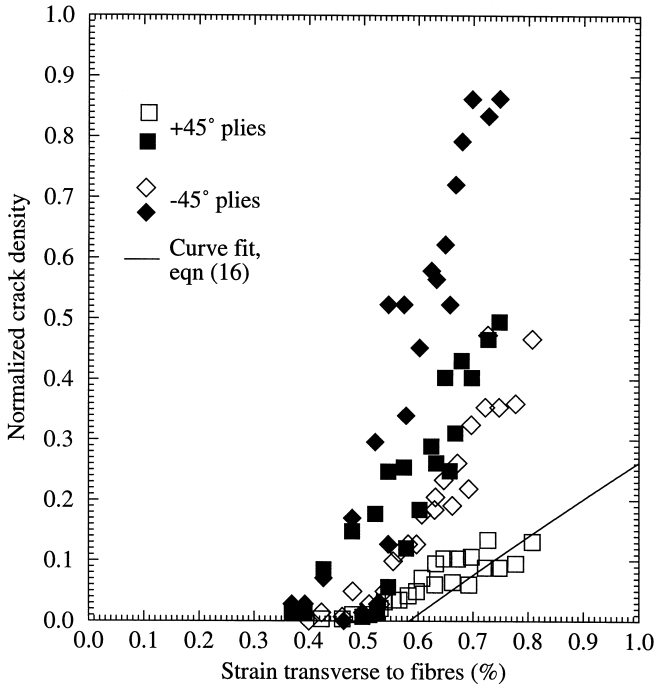

Fig. 16. Crack densities as functions of the applied strains transverse to the fibres in the separate plies for the $(0_n^\circ/+45_n^\circ/+45_n^\circ)_S$ ($n = 1, 2$) laminates. The hollow symbols indicate the experimental results for the $(0^\circ/+45^\circ/-45^\circ)_S$ and the filled symbols represent the experimentally measured crack densities of the $(0_2^\circ/+45_2^\circ/-45_2^\circ)_S$ laminates. The solid line indicates the corresponding crack evolution for the cross-ply laminates according to Fig. 11 and eqn (16).

and the $(0_n^\circ/+45_n^\circ/-45_n^\circ)_S$ laminates is presented in Fig. 17. The simulated stress levels are considerably higher than the experimentally achieved ones. The delaminations commented upon above are partly the reason for the large discrepancies. The differences between the adopted and the actual resistance curves of course also contribute to the less successful outcome of the simulations.

As can be seen in Fig. 16, the matrix crack evolution is considerably faster than indicated by the used resistance curve represented by the solid line for the $(0_n^\circ/+45_n^\circ/-45_n^\circ)_S$ laminates. From the damage progression of the quasi-isotropic $(0_n^\circ/90_n^\circ/+45_n^\circ/-45_n^\circ)_S$ laminates presented in Fig. 15, it is seen that the agreement between the assumed and the actual damage is not so bad in this case. This fact is reflected in Fig. 17 as smaller differences between the predictions and the actual values for the $(0_n^\circ/90_n^\circ/+45_n^\circ/-45_n^\circ)_S$ than for the $(0_n^\circ/+45_n^\circ/-45_n^\circ)_S$ laminates.

5.3. Matrix crack evolution in bending

The crack densities of the bending specimens are presented in Fig. 18 for both the $(90_2^\circ/0_2^\circ/-45_2^\circ/+45_2^\circ)_S$ laminates and the $(90_2^\circ/-45_2^\circ/+45_2^\circ)_S$ laminates. For these laminates, cracking occurred only in the surface 90° layers. Each specimen was bent twice, in order to produce cracks in tension in the 90° plies on both sides of the laminates. The results from the first bending

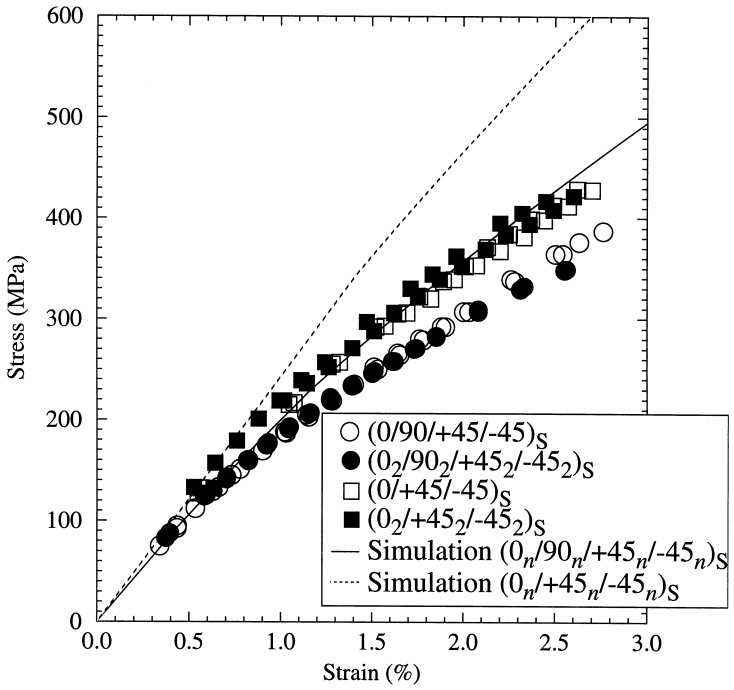

Fig. 17. The stress–strain behaviour of the tested $(0_n^\circ/90_n^\circ/+45_n^\circ/+45_n^\circ)_S$ and $(0_n^\circ/+45_n^\circ/-45_n^\circ)_S$ laminates. The experimental results are indicated by the symbols and the simulations performed by use of eqns (11)–(13) and (16) are represented by a thin solid line and a thick solid line for the $(0_n^\circ/90_n^\circ/+45_n^\circ/-45_n^\circ)_S$ and the $(0_n^\circ/+45_n^\circ/-45_n^\circ)_S$ laminates, respectively.

are indicated by hollow symbols and the crack evolution from the second bending of the specimens are shown by the filled symbols. There is no systematic difference between the hollow symbols and the filled symbols. An evident difference prevails, however, between the results for the different laminate types. The cracks in the $(90_2^\circ/-45_2^\circ/+45_2^\circ)_S$ appear at the lower average ply strains, and their amount increases faster with the applied strain than that of the cracks in the quasi-isotropic $(90_2^\circ/0_2^\circ/-45_2^\circ/+45_2^\circ)_S$ laminates. In this context, it might be noted that in the $(90_2^\circ/-45_2^\circ/+45_2^\circ)_S$ laminates, the 90° plies have as neighbours -45° plies, which are weaker in the longitudinal direction than the 0° plies adjacent to the 90° plies in the quasi-isotropic specimens.

The results of a simulation of the load–deformation curves of the specimens tested in bending are presented in Fig. 19. The simulated moments per unit length have been adjusted to fit the stiffnesses of the virgin laminates. The matrix crack evolution for the bending specimens seen in Fig. 19 show that the agreement between predicted and actual damage is fairly good for the $(90_2^\circ/-45_2^\circ/+45_2^\circ)_S$ laminates and less good for the $(90_2^\circ/0_2^\circ/-45_2^\circ/+45_2^\circ)_S$ laminates. Since the stiffness reductions for the bending specimens are relatively small and there is some scatter in the experimental data, both the simulated lines in Fig. 19 are still within the scatter band of the experiments.

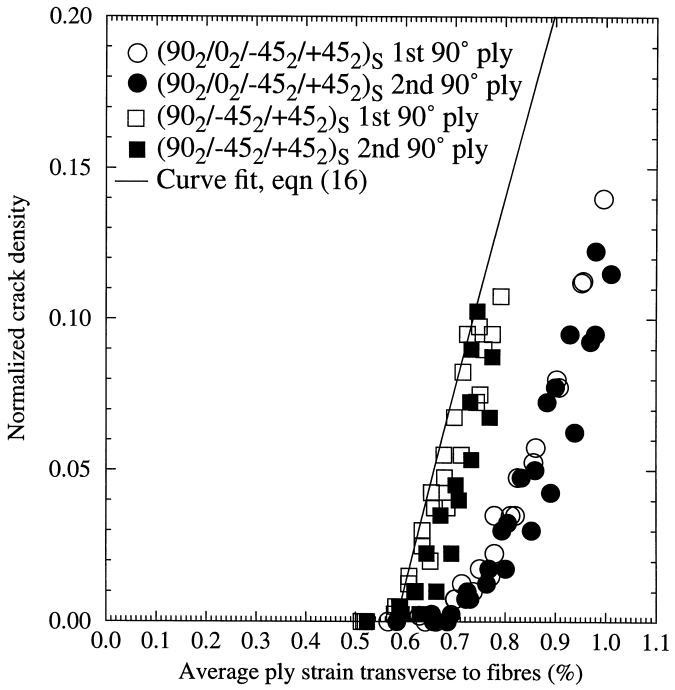

Fig. 18. The matrix crack density evolution vs the applied 90° ply average strain for the $(90_2^\circ/0_2^\circ/-45_2^\circ/+45_2^\circ)_S$ and the $(90_2^\circ/-45_2^\circ/+45_2^\circ)_S$ bending specimens. The hollow symbols indicate the results where there are cracks on only one side of the specimens. The filled symbols represent the stiffnesses of the specimens when containing cracks in the 90° plies on both sides, that is after having been bent twice. The solid line indicates the matrix crack progression characteristics of the cross-ply laminates according to eqn (16).

6. Conclusions

Experimental data from an investigation concerning matrix crack initiation and progression in glass/epoxy laminates subjected to bending and extension have been presented. In order to obtain data for different ply angles and varying stacking sequences, three types of laminates were tested in extension. These were $(0^\circ/90_n^\circ)_S$ cross-ply laminates, $(0_n^\circ/90_n^\circ/+45_n^\circ/-45_n^\circ)_S$ quasi-isotropic laminates and $(0_n^\circ/+45_n^\circ/-45_n^\circ)_S$ laminates. In the bending tests, experiments were limited to two types of laminates, namely $(90_2^\circ/0_2^\circ/-45_2^\circ/+45_2^\circ)_S$ and $(90_2^\circ/-45_2^\circ/+45_2^\circ)_S$. The recorded reductions in elastic properties in bending and extension were compared to a previously developed analytic model, and the agreement was reasonably good in all cases under consideration for the stiffnesses and in-plane Poisson's ratios. The experimentally measured longitudinal to transverse bending ratios, however, showed considerable discrepancies in comparison to the analytic results.

During the extensional tests, cracks occurred in laminates of basically two different lay-up angles, that is in plies with the fibres inclined 90 and 45°, respectively, to the longitudinal direction of the specimens. With the purpose of acquiring some knowledge of the crack initiation process, the ply stresses and strains were studied at the discovery of the first matrix crack in the considered ply. It was seen, from the rather limited set of data available, that the stress or strain normal to

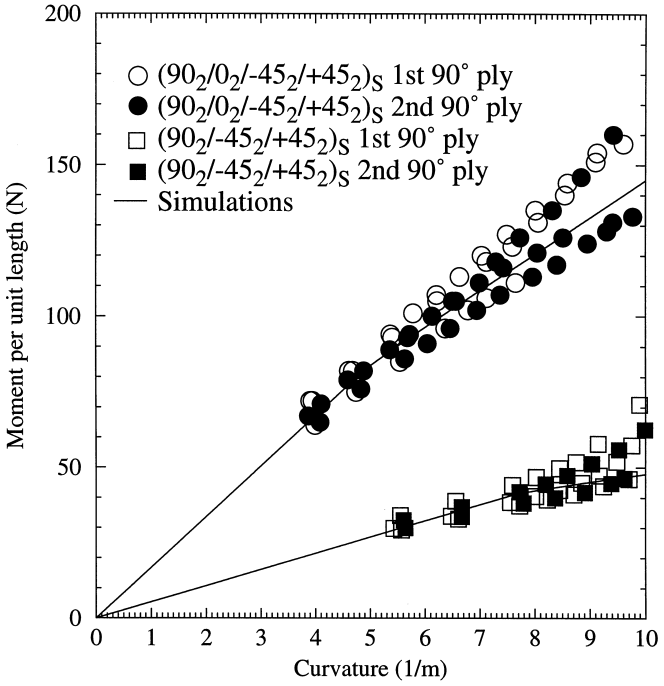

Fig. 19. The load-deformation behaviour of the $(90_2^\circ/0_2^\circ/-45_2^\circ/+45_2^\circ)_S$ and the $(90_2^\circ/-45_2^\circ/+45_2^\circ)_S$ laminates tested in bending. The experimental results are indicated by the symbols and the simulations performed by use of eqns (11)–(13) and (16) are represented by solid lines. The hollow symbols indicate the results where there are cracks on only one side of the specimens. The filled symbols represent the stiffnesses of the specimens when containing cracks in the 90° plies on both sides, that is after having been bent twice.

the fibres played a more important role than the shear stress or strain along the fibres. The present tests thus imply that the major crack initiation mechanism is of mode I type.

For the pursued damage process, an energy release rate criterion and a transverse strain criterion for matrix crack evolution were evaluated. A visualization showed a marked scatter of the energy release rates related to the crack density for the tested cross-ply laminates of different ply thicknesses. This conforms with the observations of Hahn et al. (1988). The energy release rates were also evaluated for the other tested laminates, resulting in similar results. The conclusions drawn from these calculations were that the presented expression for the energy release rate is not suitable for use as a critical crack progression parameter for the considered glass/epoxy material. It should also be noted that the energy release rates calculated in the present work contain the contributions from both the mode I and the mode II type stresses. For the cross-ply laminates, only the mode I component of stress is active, though.

The poor results which were achieved by use of an energy release rate based criterion for matrix cracking can be related to the concept of initial flaw size mentioned above. If, for the present glass/epoxy material, the initial flaw size is smaller than the smallest of the investigated ply thicknesses, then the influence of the ply thickness on the cracking process would be weak. The cracking of different ply thicknesses would then take place at the same stress or strain, since the

initial flaws of the dissimilar ply thicknesses would be of basically the same size. The results can also be disturbed by delaminations forming along with the matrix cracks. The amounts of delaminations discovered were however almost vanishing for the considered cross-ply laminates.

Turning to the other crack progression controlling parameter under consideration, the amount of matrix cracking in the cross-ply laminates proved to have a strong correlation to the strain transverse to fibres. The effects of different ply thicknesses were visible, but not very strong. Encouraged by these results, the ply strains transverse to the fibres and their relation to the amount of cracking were investigated also for the $(0_n^\circ/90_n^\circ/+45_n^\circ/-45_n^\circ)_S$ quasi-isotropic laminates and the $(0_n^\circ/+45_n^\circ/-45_n^\circ)_S$ laminates. The success in this generalization of the results from the cross-ply laminates was limited. In the laminates containing 45° plies, delaminations will play an active part in the damage process, which affects also the matrix crack evolution. A second complication is the interaction between matrix cracks of neighbouring plies. The stress concentrations at the matrix crack tips in one ply will then promote the formation of cracks in adjacent plies. Damage evolution was simulated using the ply strain transverse to the fibres as a critical parameter.

In the present investigation, the flexural properties of composite laminates were investigated at rather low curvatures, resulting in quite modest crack densities. It would be preferable to carry out further bending tests where a higher degree of bending can be obtained. It would also be of interest to examine laminates with thinner plies than in the present investigations in order to be able to capture the thickness effects observed by other researchers. The lack of thickness effects found in the present work, however, does not oppose the results found by others. It indicates that the initial flaw size for the present material is smaller than the smallest ply thickness studied.

The criteria for matrix crack initiation and progression examined in the present work cannot be said to be generally applicable. Having arrived with a reliable criterion for matrix crack evolution, however, a valuable development would be its implementation in an existing general purpose finite element code.

Appendix A

In the present Appendix, explicit expressions for the strain energy $w_{(c)}$ per unit area and for the vector of generalized forces per unit length $\boldsymbol{P}$ of the cracked laminate will be presented. The reduced thermoelastic properties used in eqns (9) and (15) will also be explicitly expressed, and the method used for the derivation of these in the work by Adolfsson and Gudmundson (1997) will be briefly illuminated.

Consider an uncracked laminate according to Section 2.1 of the present work. The elastic energy w_0 per unit area that is stored in the uncracked laminate subjected to a prescribed generalized homogeneous extension $\boldsymbol{e}$ and change in temperature ΔT may be written as

$$w_0 = \frac{1}{2}(\boldsymbol{e}-\boldsymbol{a}\Delta T)^{\mathrm{T}}\boldsymbol{C}(\boldsymbol{e}-\boldsymbol{a}\Delta T) + \sum_{k=1}^{N} f^k(\Delta T, \boldsymbol{\sigma}^{k(\mathrm{R})}), \tag{A1}$$

where $\boldsymbol{C}$ represents the 6×6 laminate effective stiffness matrix composed of the 3×3 stiffness matrices from eqn (2). The functions $f^k(\Delta T, \boldsymbol{\sigma}^{k(\mathrm{R})})$ take into account the energy stored in the laminate due to interlaminar constraints, also when $\boldsymbol{e}-\boldsymbol{a}\Delta T = \boldsymbol{0}$. The reduction in elastic energy

resulting from the presence of cracks should be expressible in terms of the applied deformation $\boldsymbol{e}$. The elastic energy for the cracked laminate can be obtained from a superposition of (i) the energy of the uncracked laminate from eqn (A1) and (ii) the change in elastic energy associated with the release of the stresses on the prospective crack surfaces. Problem two of the superposition thus corresponds to the application, with reversed sign, of the stresses calculated for the uncracked laminate onto the prospective crack surfaces under vanishing global displacements. As shown by Gudmundson and Östlund (1992), the coupling terms between problems (i) and (ii) vanish.

Consider now the second problem of the superposition. Regard a single matrix crack in a typical ply k of the laminate according to Section 2.2. The crack is loaded in the local Y_1^k-and Y_2^k-directions corresponding to mode III and mode I load types, respectively. The linearly varying in-plane ply stress $\boldsymbol{\sigma}^k$ is projected onto the prospective crack plane of ply k to form the 2×1 in-plane traction vectors $\boldsymbol{\tau}_{\mathrm{E}}^k$ and $\boldsymbol{\tau}_{\mathrm{B}}^k$ defined as

$$\begin{aligned}\boldsymbol{\tau}_{\mathrm{E}}^k &= \boldsymbol{N}^k\boldsymbol{Q}^k(\boldsymbol{\varepsilon}+z^k\boldsymbol{\kappa}-\boldsymbol{\alpha}^k\Delta T)+\boldsymbol{N}^k\boldsymbol{\sigma}_{\mathrm{E}}^{k(\mathrm{R})},\\ \boldsymbol{\tau}_{\mathrm{B}}^k &= \frac{t^k}{2}\boldsymbol{N}^k\boldsymbol{Q}^k\boldsymbol{\kappa}+\boldsymbol{N}^k\boldsymbol{\sigma}_{\mathrm{B}}^{k(\mathrm{R})},\end{aligned} \tag{A2}$$

where $\boldsymbol{\sigma}_{\mathrm{E}}^{k(\mathrm{R})}$ and $\boldsymbol{\sigma}_{\mathrm{B}}^{k(\mathrm{R})}$ are the vectors of averages and amplitudes, respectively, of an assumed linearly varying residual stress vector in ply k. The vector $\boldsymbol{\tau}_{\mathrm{E}}^k$ thus represents the average tractions in the ply whereas the linearly varying fraction of the tractions is contained in the vector $\boldsymbol{\tau}_{\mathrm{B}}^k$. The matrix $\boldsymbol{N}^k$ is defined from the constant unit normal vector $\boldsymbol{n}^k$ of the crack surfaces of ply k and reads

$$\boldsymbol{N}^k=\begin{pmatrix} n_1^k & 0 & n_2^k\\ 0 & n_2^k & n_1^k\end{pmatrix}. \tag{A3}$$

Introducing the 4×4 matrices $\boldsymbol{\beta}^{kl}$ and the 4×1 vectors $\boldsymbol{\tau}^k$ as

$$\boldsymbol{\beta}^{kl}=\begin{pmatrix}\boldsymbol{\beta}_{\mathrm{EE}}^{kl} & \boldsymbol{\beta}_{\mathrm{EB}}^{kl}\\ \boldsymbol{\beta}_{\mathrm{BE}}^{kl} & \boldsymbol{\beta}_{\mathrm{BB}}^{kl}\end{pmatrix}\quad \boldsymbol{\tau}^k=\begin{pmatrix}\boldsymbol{\tau}_{\mathrm{E}}^k\\ \boldsymbol{\tau}_{\mathrm{B}}^k\end{pmatrix}, \tag{A4}$$

the work ΔW^k done by the tractions $\boldsymbol{\tau}^k$ on all crack surfaces in ply k may be expressed as

$$\Delta W^k=\frac{t^k\sqrt{l^k}}{2}(\boldsymbol{\tau}^k)^{\mathrm{T}}\sum_{l=1}^{N}t^l\sqrt{l^l}\boldsymbol{\beta}^{kl}\boldsymbol{\tau}^l, \tag{A5}$$

where l^k is the total crack length in the ply k. The 2×2 submatrices $\boldsymbol{\beta}_m^{kl}$ ($m=\mathrm{EE},\mathrm{EB},\mathrm{BE},\mathrm{BB}$) of the $\boldsymbol{\beta}^{kl}$—matrices will be defined in the next section. The apparently arbitrarily chosen lengths in eqn (A5) are introduced in order to enable convenient subsequent derivations. The length l^k is connected to the laminate in-plane area A and to the crack density ρ^k through

$$l^k=\frac{A\rho^k}{t^k}. \tag{A6}$$

The contributions to the total crack surface work from all plies may now be added to obtain the total change in elastic energy Δw per unit area as

$$\Delta w = \frac{1}{2}\sum_{k=1}^{N}\sum_{l=1}^{N}\sqrt{t^k\rho^k t^l\rho^l}(\boldsymbol{\tau}^k)^{\mathrm{T}}\boldsymbol{\beta}^{kl}\boldsymbol{\tau}^l. \tag{A7}$$

The total elastic energy $w_{(c)}$ per unit area for the cracked laminate is calculated by subtracting the crack surface work Δw per unit area in eqn (A7) from the energy w_0 per unit area valid for the uncracked laminate, so

$$w_{(c)} = \frac{1}{2}\left((\boldsymbol{e}-\boldsymbol{a}\Delta T)^{\mathrm{T}}\boldsymbol{C}(\boldsymbol{e}-\boldsymbol{a}\Delta T) - \sum_{k=1}^{N}\sum_{l=1}^{N}\sqrt{t^k\rho^k t^l\rho^l}(\boldsymbol{\tau}^k)^{\mathrm{T}}\boldsymbol{\beta}^{kl}\boldsymbol{\tau}^l\right) + \sum_{k=1}^{N} f^k(\Delta T, \boldsymbol{\sigma}^{k(\mathrm{R})}). \tag{A8}$$

For a cracked laminate in general, the following expression describes the elastic energy, provided that both thermal expansion and eigenstrains $\boldsymbol{e}^{(\mathrm{R})}$ due to residual stresses are taken into account:

$$w_{(c)} = \frac{1}{2}(\boldsymbol{e}-\boldsymbol{a}_{(c)}\Delta T-\boldsymbol{e}^{(\mathrm{R})})^{\mathrm{T}}\boldsymbol{C}_{(c)}(\boldsymbol{e}-\boldsymbol{a}_{(c)}\Delta T-\boldsymbol{e}^{(\mathrm{R})}) + \sum_{k=1}^{N} h^k(\Delta T, \boldsymbol{\sigma}^{k(\mathrm{R})}). \tag{A9}$$

Letters with subscript (c) indicate properties of the cracked laminate. Since eqns (A8) and (A9) represent two alternative ways of expressing the elastic energy of the damaged laminate, the stiffnesses, thermal expansion coefficients and eigenstrains of the cracked laminate can be obtained from an identification of terms using these two equations. To enable this, the tractions $\boldsymbol{\tau}^k$ in eqn (A8) need to be expressed in terms of the generalized strain measures and residual stresses according to eqns (A2) and (A4). Identifying then terms containing the generalized strain vector $\boldsymbol{e}$ yields the thermoelastic properties of the cracked laminate. By use of the matrices $\boldsymbol{A}_m^{kl}$, defined as

$$\boldsymbol{A}_m^{kl} = \boldsymbol{Q}^k(\boldsymbol{N}^k)^{\mathrm{T}}\boldsymbol{\beta}_m^{kl}\boldsymbol{N}^l\boldsymbol{Q}^l, \quad (m = \mathrm{EE}, \mathrm{EB}, \mathrm{BE}, \mathrm{BB}) \tag{A10}$$

the changes $\Delta\boldsymbol{C}$ and $\Delta\boldsymbol{\delta}$ in stiffnesses and thermal stress coefficients along with the apparent forces $\boldsymbol{N}^{(\mathrm{R})}$ and moments $\boldsymbol{M}^{(\mathrm{R})}$ per unit length due to the release of residual stresses are introduced as

$$\Delta\boldsymbol{C}_{\mathrm{EE}} = -\sum_{k=1}^{N}\sum_{l=1}^{N}\sqrt{t^k\rho^k t^l\rho^l}\boldsymbol{A}_{\mathrm{EE}}^{kl}, \tag{A11a}$$

$$\Delta\boldsymbol{C}_{\mathrm{EB}} = \Delta\boldsymbol{C}_{\mathrm{BE}}^{\mathrm{T}} = -\sum_{k=1}^{N}\sum_{l=1}^{N}\sqrt{t^k\rho^k t^l\rho^l}\left[z^l\boldsymbol{A}_{\mathrm{EE}}^{kl} + \frac{t^l}{2}\boldsymbol{A}_{\mathrm{EB}}^{kl}\right], \tag{A11b}$$

$$\Delta\boldsymbol{C}_{\mathrm{BB}} = -\sum_{k=1}^{N}\sum_{l=1}^{N}\sqrt{t^k\rho^k t^l\rho^l}\left[z^k z^l\boldsymbol{A}_{\mathrm{EE}}^{kl} + \frac{z^k t^l}{2}\boldsymbol{A}_{\mathrm{EB}}^{kl} + \frac{z^l t^k}{2}\boldsymbol{A}_{\mathrm{BE}}^{kl} + \frac{t^k t^l}{4}\boldsymbol{A}_{\mathrm{BB}}^{kl}\right], \tag{A11c}$$

$$\Delta\boldsymbol{\delta}_{\mathrm{E}} = \Delta\boldsymbol{C}_{\mathrm{EE}}\boldsymbol{\alpha}_{\mathrm{E}} + \Delta\boldsymbol{C}_{\mathrm{EB}}\boldsymbol{\alpha}_{\mathrm{B}} + \sum_{k=1}^{N}\sum_{l=1}^{N}\sqrt{t^k\rho^k t^l\rho^l}\boldsymbol{A}_{\mathrm{EE}}^{kl}\boldsymbol{\alpha}^l, \tag{A11d}$$

$$\Delta\boldsymbol{\delta}_{\mathrm{B}} = \Delta\boldsymbol{C}_{\mathrm{BE}}\boldsymbol{\alpha}_{\mathrm{E}} + \Delta\boldsymbol{C}_{\mathrm{BB}}\boldsymbol{\alpha}_{\mathrm{B}} + \sum_{k=1}^{N}\sum_{l=1}^{N}\sqrt{t^k\rho^k t^l\rho^l}\left[z^k\boldsymbol{A}_{\mathrm{EE}}^{kl} + \frac{t^k}{2}\boldsymbol{A}_{\mathrm{BE}}^{kl}\right]\boldsymbol{\alpha}^l, \tag{A11e}$$

$$\boldsymbol{N}^{(\mathrm{R})} = \sum_{k=1}^{N}\sum_{l=1}^{N}\sqrt{t^k\rho^k t^l\rho^l}[\boldsymbol{A}^{kl}_{\mathrm{EE}}(\boldsymbol{Q}^l)^{-1}\boldsymbol{\sigma}^{l(\mathrm{R})}_{\mathrm{E}} + \boldsymbol{A}^{kl}_{\mathrm{EB}}(\boldsymbol{Q}^l)^{-1}\boldsymbol{\sigma}^{l(\mathrm{R})}_{\mathrm{B}}], \tag{A11f}$$

$$\boldsymbol{M}^{(\mathrm{R})} = \sum_{k=1}^{N}\sum_{l=1}^{N}\sqrt{t^k\rho^k t^l\rho^l}\left[\left(z^k\boldsymbol{A}^{kl}_{\mathrm{EE}} + \frac{t^k}{2}\boldsymbol{A}^{kl}_{\mathrm{BE}}\right)(\boldsymbol{Q}^l)^{-1}\boldsymbol{\sigma}^{l(\mathrm{R})}_{\mathrm{E}} + \left(z^k\boldsymbol{A}^{kl}_{\mathrm{EB}} + \frac{t^k}{2}\boldsymbol{A}^{kl}_{\mathrm{BB}}\right)(\boldsymbol{Q}^l)^{-1}\boldsymbol{\sigma}^{l(\mathrm{R})}_{\mathrm{B}}\right]. \tag{A11g}$$

The compliances, thermal expansion coefficients and generalized eigenstrains of the cracked composite laminate resulting from the identification between eqns (A8) and (A9) then read

$$\boldsymbol{S}_{\mathrm{EE(c)}} = [\boldsymbol{C}_{\mathrm{EE}} + \Delta\boldsymbol{C}_{\mathrm{EE}} - (\boldsymbol{C}_{\mathrm{EB}} + \Delta\boldsymbol{C}_{\mathrm{EB}})(\boldsymbol{C}_{\mathrm{BB}} + \Delta\boldsymbol{C}_{\mathrm{BB}})^{-1}(\boldsymbol{C}_{\mathrm{BE}} + \Delta\boldsymbol{C}_{\mathrm{BE}})]^{-1}, \tag{A12a}$$

$$\boldsymbol{S}_{\mathrm{EB(c)}} = \boldsymbol{S}^{\mathrm{T}}_{\mathrm{BE(c)}} = -\boldsymbol{S}_{\mathrm{EE(c)}}(\boldsymbol{C}_{\mathrm{EB}} + \Delta\boldsymbol{C}_{\mathrm{EB}})(\boldsymbol{C}_{\mathrm{BB}} + \Delta\boldsymbol{C}_{\mathrm{BB}})^{-1}, \tag{A12b}$$

$$\boldsymbol{S}_{\mathrm{BB(c)}} = (\boldsymbol{C}_{\mathrm{BB}} + \Delta\boldsymbol{C}_{\mathrm{BB}})^{-1} + \boldsymbol{S}_{\mathrm{BE(c)}}\boldsymbol{S}^{-1}_{\mathrm{EE(c)}}\boldsymbol{S}_{\mathrm{EB(c)}}, \tag{A12c}$$

$$\boldsymbol{\alpha}_{\mathrm{E(c)}} = \boldsymbol{\alpha}_{\mathrm{E}} - \boldsymbol{S}_{\mathrm{EE(c)}}\Delta\boldsymbol{\delta}_{\mathrm{E}} - \boldsymbol{S}_{\mathrm{EB(c)}}\Delta\boldsymbol{\delta}_{\mathrm{B}}, \tag{A12d}$$

$$\boldsymbol{\alpha}_{\mathrm{B(c)}} = \boldsymbol{\alpha}_{\mathrm{B}} - \boldsymbol{S}_{\mathrm{BE(c)}}\Delta\boldsymbol{\delta}_{\mathrm{E}} - \boldsymbol{S}_{\mathrm{BB(c)}}\Delta\boldsymbol{\delta}_{\mathrm{B}}, \tag{A12e}$$

$$\boldsymbol{\varepsilon}^{(\mathrm{R})} = \boldsymbol{S}_{\mathrm{EE(c)}}N^{(\mathrm{R})} + \boldsymbol{S}_{\mathrm{EB(c)}}\boldsymbol{M}^{(\mathrm{R})}, \tag{A12f}$$

$$\boldsymbol{\kappa}^{(\mathrm{R})} = \boldsymbol{S}_{\mathrm{BE(c)}}\boldsymbol{N}^{(\mathrm{R})} + \boldsymbol{S}_{\mathrm{BB(c)}}\boldsymbol{M}^{(\mathrm{R})}. \tag{A12g}$$

The expression in eqn (A8) may be explicitly differentiated with respect to the vector of generalized strains $\boldsymbol{e}$ to obtain an expression for the load vector $\boldsymbol{P}$ for the cracked laminate from eqn (10). To enable this, the tractions $\boldsymbol{\tau}^k$ in eqn (A8) need to be replaced by the generalized strain measures and residual stresses according to eqns (A2) and (A4). As a result, the vectors $\boldsymbol{N}$ and $\boldsymbol{M}$ of forces and moments per unit length for the cracked laminate read

$$\boldsymbol{N} = \boldsymbol{C}_{\mathrm{EE}}\boldsymbol{\varepsilon} + \boldsymbol{C}_{\mathrm{EB}}\boldsymbol{\kappa} - (\boldsymbol{C}_{\mathrm{EE}}\boldsymbol{\alpha}_{\mathrm{E}} + \boldsymbol{C}_{\mathrm{EB}}\boldsymbol{\alpha}_{\mathrm{B}})\Delta T - \sum_{k=1}^{N}\sum_{l=1}^{N}\sqrt{t^k\rho^k t^l\rho^l}\boldsymbol{Q}^k(\boldsymbol{N}^k)^{\mathrm{T}}[\boldsymbol{\beta}^{kl}_{\mathrm{EE}}\boldsymbol{\tau}^l_{\mathrm{E}} + \boldsymbol{\beta}^{kl}_{\mathrm{EB}}\boldsymbol{\tau}^l_{\mathrm{B}}] \tag{A13}$$

and

$$\boldsymbol{M} = \boldsymbol{C}_{\mathrm{BE}}\boldsymbol{\varepsilon} + \boldsymbol{C}_{\mathrm{BB}}\boldsymbol{\kappa} - (\boldsymbol{C}_{\mathrm{BE}}\boldsymbol{\alpha}_{\mathrm{E}} + \boldsymbol{C}_{\mathrm{BB}}\boldsymbol{\alpha}_{\mathrm{B}})\Delta T - \sum_{k=1}^{N}\sum_{l=1}^{N}\sqrt{t^k\rho^k t^l\rho^l}\boldsymbol{Q}^k(\boldsymbol{N}^k)^{\mathrm{T}}\left[z^k(\boldsymbol{\beta}^{kl}_{\mathrm{EE}}\boldsymbol{\tau}^l_{\mathrm{E}} + \boldsymbol{\beta}^{kl}_{\mathrm{EB}}\boldsymbol{\tau}^l_{\mathrm{B}}) + \frac{t^k}{2}(\boldsymbol{\beta}^{kl}_{\mathrm{BE}}\boldsymbol{\tau}^l_{\mathrm{E}} + \boldsymbol{\beta}^{kl}_{\mathrm{BB}}\boldsymbol{\tau}^l_{\mathrm{B}})\right]. \tag{A14}$$

A simple model for matrix crack closure which was successfully used by Adolfsson and Gudmundson (1994) may be applied to eqns (A13) and (A14). The criterion for crack closure in ply k is then that the average traction component in the local Y^k_2-direction is negative. In that case, the contributions to the reductions in $\boldsymbol{N}$ and $\boldsymbol{M}$ from ply k vanish. By expressing the vectors of ply tractions $\boldsymbol{\tau}^k_{\mathrm{E}}$ and $\boldsymbol{\tau}^k_{\mathrm{B}}$ in the applied loads $\boldsymbol{e}$ and ΔT according to eqn (A2), and using the expressions for the thermoelastic properties seen in eqns (A11) and (A12), eqns (A13) and (A14) may be transformed into the equality seen in eqn (10).

A detailed derivation of the sub-matrices $\boldsymbol{\beta}^{kl}_{\mathrm{EE}}$, $\boldsymbol{\beta}^{kl}_{\mathrm{EB}}$, $\boldsymbol{\beta}^{kl}_{\mathrm{BE}}$ and $\boldsymbol{\beta}^{kl}_{\mathrm{BB}}$ used in eqns (A10)–(A14) may be found in the work of Adolfsson and Gudmundson (1997). The resulting expressions for these matrices will be given below. The matrix components are derived from stress intensity factors for problems closely related to the laminate matrix crack problem. As a result, the matrix components can be expressed in terms of integrals over the crack length. The integrands contain expressions for the utilized stress intensity factors. In order to avoid time consuming evaluation of the integrals for each calculation of effective properties, the integrals have been analytically evaluated if possible. The other integrals were numerically evaluated and expressions were fitted to them. The curve fit parameters found in Tables A1 and A2 are hence universal properties, independent of material properties, and reflect only the dependence on the ply crack densities. In the following expressions,

Table A1
The curve fit parameters used in eqns (A15) and (A16) determining the crack density dependence of the components of the matrices $\boldsymbol{\beta}^{kk(\mathrm{i})}_{\mathrm{EE}}$ and $\boldsymbol{\beta}^{kk(\mathrm{i})}_{\mathrm{BB}}$. Values taken from Adolfsson and Gudmundson (1997)

j	a_j	b_j	c_j
1	0.63666	3.40409	1.65364
2	0.51806	−1.50821	0.87842
3	0.51695	−0.37842	10.61342
4	−1.04897	−3.62256	−135.67488
5	8.95572	−101.24283	747.53392
6	−33.09444	481.87306	−2236.32476
7	74.32002	−916.59087	3772.21227
8	−103.06411	898.56902	−3604.17159
9	73.60337	−452.85541	1827.29629
10	−20.34326	93.35216	−383.01680

Table A2
The curve fit parameters used in eqns (A17), (A18) and (A19) determining the crack density dependence of the components of the matrices $\boldsymbol{\beta}^{kk(\mathrm{s})}_{m}$ (m = EE, EB, BE, BB). Values taken from Adolfsson and Gudmundson (1997)

j	d_j	e_j	f_j	g_j	h_j
1	0.25256	−0.29208	−0.03521	2.00624	0.86388
2	0.27079	8.70026	0.97809	−2.57041	−2.87984
3	−0.49814	−82.11858	−7.58709	31.41892	34.19264
4	8.62962	479.23609	44.52217	−175.60882	−167.57885
5	−51.24655	−1633.39371	−150.85828	547.80573	458.21598
6	180.96305	3497.22398	333.94609	−1114.56953	−667.14207
7	−374.29813	−4751.26789	−487.71444	1494.40862	400.51994
8	449.59474	3954.62876	471.87242	−1256.18363	109.75154
9	−286.51016	−1835.18896	−273.59771	594.64188	−252.27544
10	73.84223	363.47237	69.47435	−120.34912	87.33293

a superscript (i) indicates interior cracks, and a superscript (s) indicates surface cracks. For interior cracks, the following matrix components result:

$$\beta^{kk(\mathrm{i})}_{11(\mathrm{EE})} = \frac{\pi}{2}\gamma_1^k \frac{8}{(\pi\rho^k)^2}\ln\left[\cosh\left(\frac{\pi\rho^k}{2}\right)\right],$$

$$\beta^{kk(\mathrm{i})}_{22(\mathrm{EE})} = \frac{\pi}{2}\gamma_2^k \sum_{j=1}^{10}\frac{a_j}{(1+\rho^k)^j} \tag{A15}$$

for the component associated with pure extension and

$$\beta^{kk(\mathrm{i})}_{11(\mathbf{BB})} = \frac{\pi}{16}\gamma_1^k \sum_{j=1}^{10}\frac{b_j}{(1+\rho^k)^j},$$

$$\beta^{kk(\mathrm{i})}_{22(\mathbf{BB})} = \frac{\pi}{16}\gamma_2^k \sum_{j=1}^{10}\frac{c_j}{(1+\rho^k)^j} \tag{A16}$$

for the components which must be added to take bending into account. The curve fit parameters a_j, b_j and c_j are found in Table A1. The matrices $\boldsymbol{\beta}^{kk(\mathrm{s})}_{\mathrm{EB}}$ and $\boldsymbol{\beta}^{kk(\mathrm{s})}_{\mathrm{BE}}$ both vanish, as do all matrices for which $k \neq l$.

For surface cracks there exists a coupling between the components of the traction vector associated with extension and bending. Care must also be devoted to the location of the crack tip in relation to the peak stress, which is insignificant for interior cracks. The explicit expressions for the matrix components for surface cracks are

$$\beta^{kk(\mathrm{s})}_{11(\mathrm{EE})} = \pi\gamma_1^k \frac{8}{(2\pi\rho^k)^2}\ln\left[\cosh(\pi\rho^k)\right],$$

$$\beta^{kk(\mathrm{s})}_{22(\mathrm{EE})} = 1.1215^2\pi\gamma_2^k \sum_{j=1}^{10}\frac{d_j}{(1+\rho^k)^j} \tag{A17}$$

for the purely extensional load. Incorporating also the fraction of the traction corresponding to bending, the following equations result:

$$\beta^{kk(\mathrm{s})}_{11(\mathrm{EB})} = \beta^{kk(\mathrm{s})}_{11(\mathrm{BE})} = -\frac{3\pi-8}{3}\gamma_1^k \sum_{j=1}^{10}\frac{e_j}{(1+\rho^k)^j},$$

$$\beta^{kk(\mathrm{s})}_{22(\mathrm{EB})} = \beta^{kk(\mathrm{s})}_{22(\mathrm{BE})} = -0.2364\pi\gamma_2^k \sum_{j=1}^{10}\frac{f_j}{(1+\rho^k)^j} \tag{A18}$$

and

$$\beta^{kk(\mathrm{s})}_{11(\mathbf{BB})} = \frac{3\pi^2-16\pi+24}{3\pi}\gamma_1^k \sum_{j=1}^{10}\frac{g_j}{(1+\rho^k)^j},$$

$$\beta^{kk(\mathrm{s})}_{22(\mathbf{BB})} = 0.1481\pi\gamma_2^k \sum_{j=1}^{10}\frac{h_j}{(1+\rho^k)^j}. \tag{A19}$$

The fitted parameters d_j, e_j, f_j, g_j and h_j are found in Table A2. For high crack densities, matrices which correspond to an infinite crack density may be applicable. These matrices are explicitly

$$\beta^{kk(\mathrm{inf})}_{11(\mathrm{EE})} = \frac{2\gamma_1^k}{\rho^k},$$

$$\beta^{kk(\mathrm{inf})}_{22(\mathrm{EE})} = \frac{\gamma_2^k}{\rho^k} \tag{A20}$$

and

$$\beta^{kk(\mathrm{inf})}_{11(\mathrm{BB})} = \frac{2\gamma_1^k}{3\rho^k},$$

$$\beta^{kk(\mathrm{inf})}_{22(\mathrm{BB})} = \frac{\gamma_2^k}{3\rho^k}. \tag{A21}$$

The matrix components given in eqns (A20) and (A21) hence also give lower bounds for the elastic moduli of cracked laminates. The components of the $\boldsymbol{\beta}^{kk}$ matrices given above are valid in the local Y_1^k, Y_2^k, Y_3^k coordinate system in ply k. For the calculation of the laminate properties, the matrices of the different plies need to be transformed to a common coordinate system.

Appendix B

In the present Appendix, the device which enables the introduction of a constant and pure bending moment over the entire length of the bending specimens will be briefly described. The design of the apparatus is shown schematically in Fig. B1. The load is introduced using a system of wires and wheels, which is self-adjusting to sustain symmetry. The force P is applied to the wheels at the top and bottom of Fig. B1. In the present experiments, displacement control was used so that the increase in distance d between the two wheels is utilized as the loading parameter. The specimen of length s to be tested is attached to two rigid beams of length a, through which the bending moment is introduced via the wires that run over the wheels and are connected to the rigid beams. In order to calculate the moment which is applied to the test specimen, the angle θ needs to be known. This angle can be calculated by use of two geometrical observations. The original length L_0 of one of the wires is

$$L_0 = \frac{2b+s}{\cos\varphi_0} + r(\pi - 2\varphi_0) + 2r\tan\varphi_0. \tag{B1}$$

When the load has been applied, the increased wire length L can be written as

$$L = \frac{2b+d+s-a\sin\theta}{\cos\varphi} + r(\pi - 2\varphi) + 2r\tan\varphi. \tag{B2}$$

Further, for small strains in the wire it holds that $L = (1+\varepsilon)L_0$, where $\varepsilon = P/(2EA\cos\varphi)$, which leads to the following equation:

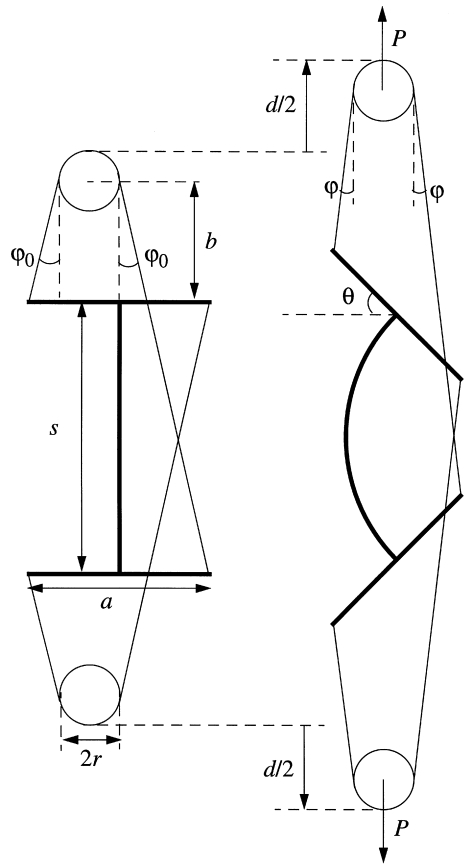

Fig. B1. A schematic of the device used for the bending tests. The specimen of length s to be tested is clamped to two rigid beams, each of length a. The load P is introduced via a controlled displacement $d/2$ of each of the two wheels of the apparatus.

$$L = \left(1 + \frac{P}{2EA\cos\varphi}\right) L_0, \tag{B3}$$

where the E-modulus and the cross-sectional area of the wire have been indicated as E and A, respectively. In many cases, the increases in length of the wires can be neglected. This is true in particular when testing thin composite laminates, which are weak in bending and hence do not require large forces. The length a of one of the rigid beams may be expressed as

$$a = (2b + s)\tan\varphi_0 + \frac{2r}{\cos\varphi_0}. \tag{B4}$$

In the deformed configuration, this distance can be written as

$$a = \frac{(2b + d + s)\tan\varphi + \dfrac{2r}{\cos\varphi}}{\cos\theta + \sin\theta\tan\varphi}. \tag{B5}$$

From a combination of eqns (B1)–(B3) and (B4)–(B5), respectively, the following system of equations is obtained:

$$\frac{2b+d+s-a\sin\theta}{\cos\varphi}+r(\pi-2\varphi)+2r\tan\varphi$$
$$-\left(1+\frac{P}{2EA\cos\varphi}\right)\left(\frac{2b+s}{\cos\varphi_0}+r(\pi-2\varphi_0)+2r\tan\varphi_0\right)=0$$
$$\frac{(2b+d+s)\tan\varphi+\dfrac{2r}{\cos\varphi}}{\cos\theta+\sin\theta\tan\varphi}-\left((2b+s)\tan\varphi_0+\frac{2r}{\cos\varphi_0}\right)=0. \tag{B6}$$

The angle φ_0 can be recovered from eqn (B4). Knowing the controlled parameter d, the system of eqns (B6) may be solved to find the angles φ and θ. The moment M in the bending specimen is then calculated as

$$M=\frac{Pa}{2}\cos\theta. \tag{B7}$$

When using the described apparatus for bending tests, it is preferable to minimize the bending stiffness of the included wires, in order to achieve a behaviour as close to ideal as possible. The length s of the specimen to be tested can be arbitrarily chosen. Shorter specimens will then enable the application of a larger curvature. In the present investigation, the device has been used in horizontal position on a smooth surface to minimize the effects of gravity. In an upright position, frictional forces are avoided. Gravity in this case, however, induces forces that disturb the symmetry of the apparatus.

Acknowledgements

The authors wish to acknowledge Mr Hans Öberg for skilful experimental assistance and for the design of the device used in the bending tests. Dr Mårten Olsson is appreciated for fruitful discussions concerning the interpretation of experimental data. Mr Grunde Wahl thoroughly performed initial experiments in order to evaluate the edge replication technique. Thanks are also directed to Messrs Bengt Andersson, Bengt Möllerberg and Per Lagercrantz for manufacturing of experimental equipment.

References

Abrate, S., 1991. Matrix cracking in laminated composites: a review. Composites Engineering 1, 337–353.

Adolfsson, E., Gudmundson, P., 1994. Matrix crack closure effects on the thermoelastic properties of $[(0^\circ/90^\circ/+45^\circ/-45^\circ)_s]_M$ composite laminates. In: Kardomateas, G.A., Rajapakse, Y.D.S. (Eds.), Failure Mechanics in Advanced Polymeric Composites, AMD-Vol. 196. The American Society of Mechanical Engineers, New York, NY, pp. 125–140.

Adolfsson, E., Gudmundson, P., 1997. Thermoelastic properties in combined bending and extension of thin composite laminates with transverse matrix cracks. International Journal of Solids and Structures 34, 2035–2060.

Altus, E., Ishai, O., 1986. Transverse cracking and delamination interaction in the failure process of composite laminates. Composite Science and Technology 26, 59–77.

Altus, E., Ishai, O., 1990. The effect of soft interleaved layers on the combined transverse cracking/delamination mechanisms in composite laminates. Composites Science and Technology 39, 13–27.

ASTM, 1991. Standard practice for in-plane shear stress–strain response of unidirectional polymer matrix composites. ASTM D 3518/D 3518M-91. American Society for Testing and Materials, Philadelphia, PA.

ASTM, 1993. Standard test method for tensile properties of polymer-matrix composite materials. ASTM D 3039/D 3039M-93. American Society for Testing and Materials, Philadelphia, PA.

Armarinos, E.A., Sriram, P., Badir, A.M., 1991. Fracture analysis of transverse crack-tip and free-edge delamination in laminated composites. In: O'Brien, T.K. (Ed.), Composite Materials: Fatigue and Fracture, vol. 3, ASTM STP 1110. American Society for Testing and Materials, Philadelphia, PA, pp. 269–286.

Aveston, J., Kelly, A., 1973. Theory of multiple fracture of fibrous composites. Journal of Materials Science 8, 352–362.

Bailey, J.E., Curtis, P.T., Parvizi, A., 1979. On the transverse cracking and longitudinal splitting behaviour of glass and carbon fibre reinforced epoxy cross ply laminates and the effect of Poisson and thermally generated strain. Proceedings of the Royal Society London A 366, 599–623.

Boniface, L., Ogin, S.L., Smith, P.A., 1991. Fracture mechanics approaches to transverse ply cracking in composite laminates. In: O'Brien, T.K. (Ed.), Composite Materials: Fatigue and Fracture, vol. 3, ASTM STP 1110. American Society for Testing and Materials, Philadelphia, PA, pp. 9–29.

Chatterjee, S.N., Wung, E.C.J., Yen, C.F., 1993. Modeling ply crack growth in laminates under combined stress states. In: Stinchcomb, W.W., Ashbaugh, N.E. (Eds.), Composite Materials: Fatigue and Fracture, vol. 4, ASTM STP 1156. American Society for Testing and Materials, Philadelphia, PA, pp. 195–217.

Crocker, L.E., Ogin, S.L., Smith, P.A., 1996. Mixed mode intra-laminar fracture in glass-epoxy laminates under quasi-static loading. In: Proceedings of ECCM-7, Realising Their Commercial Potential, vol. 1. Woodhead Publishing Ltd, Abington Hall, Cambridge, U.K.

Dvorak, G.J., Laws, N., 1986. Analysis of first ply failure in composite laminates. Engineering Fracture Mechanics 25, 763–770.

Dvorak, G.J., Laws, N., Hejazi, M., 1985. Analysis of progressive matrix cracking in composite laminates I. Thermoelastic properties of a ply with cracks. Journal of Composite Materials 19, 216–234.

Eggers, H., Goetting, H.C., Bäuml, H., 1994. Synergism between layer cracking and delaminations in multidirectional laminates of carbon fibre reinforced epoxy. Composites Science and Technology 50, 343–354.

Flaggs, D.L., 1985. Prediction of tensile matrix failure in composite materials. Journal of Composite Materials 19, 29–50.

Flaggs, D.L., Kural, M.H., 1982. Experimental determination of the in situ transverse lamina strength in graphite/epoxy laminates. Journal of Composite Materials 16, 103–116.

Fukunaga, H., Chou, T.-W., Peters, P.W.M., Schulte, K., 1984. Probabilistic failure strength analyses of graphite/epoxy cross-ply laminates. Journal of Composite Materials 18, 339–356.

Garrett, K.W., Bailey, J.E., 1977a. Multiple transverse fracture in 90° cross-ply laminates of a glass fibre-reinforced polyester. Journal of Materials Science 12, 157–168.

Garrett, K.W., Bailey, J.E., 1977b. The effect of resin failure strain on the tensile properties of glass fibre-reinforced polyester cross-ply laminates. Journal of Materials Science 12, 2189–2194.

Gudmundson, P., Östlund, S., 1992. First order analysis of stiffness reduction due to matrix cracking. Journal of Composite Materials 26, 1009–1030.

Gudmundson, P., Zang, W., 1993. An analytic model for the thermoelastic properties of composite laminates containing transverse matrix cracks. International Journal of Solids and Structures 30, 3211–3231.

Hahn, H.T., Tsai, S.W., 1974. On the behavior of composite laminates after initial failures. Journal of Composite Materials 8, 288–305.

Hahn, H.T., Han, Y.M., Kim, R.Y., 1988. Resistance curves for ply cracking in composite laminates. In: Proceedings of the 33rd International SAMPE Symposium, 7–10 March 1988, pp. 1101–1108.

Harrison, R.P., Bader, M.G., 1983. Damage development in CFRP laminates under monotonic and cyclic stressing. Fibre Science and Technology 18, 163–180.

Hashin, Z., 1985. Analysis of cracked laminates: a variational approach. Mechanics of Materials 4, 121–136.

Hashin, Z., 1987. Analysis of orthogonally cracked laminates under tension. Journal of Applied Mechanics 54, 872–879.

Hashin, Z., 1988. Thermal expansion coefficients of cracked laminates. Composites Science and Technology 31, 247–260.

Hashin, Z., 1996. Finite thermoelastic fracture criterion with application to laminate cracking analysis. Journal of the Mechanics and Physics of Solids 44, 1129–1145.

Jamison, R.D., Reifsnider, K.L., 1982. Advanced fatigue damage development in graphite epoxy laminates. Report AFWAL TR-82-3103. Virginia Polytechnic Institute and State University, Blacksburg, VA.

Jen, K.C., Sun, C.T., 1990. Matrix cracking and delamination prediction in graphite/epoxy laminates. In: Lansing, E. (Ed.), Proceedings of the American Society for Composites, Fifth Technical Conference, 12–14 June 1990. Technomic Publishing Co., MI, pp. 350–360.

Lafarie-Frenot, M.C., Hénaff-Gardin, C., 1991. Formation and growth of 90° ply fatigue cracks in carbon/epoxy laminates. Composite Science and Technology 40, 307–324.

Laws, N., Dvorak, G.J., Hejazi, M., 1983. Stiffness changes in unidirectional composites caused by crack systems. Mechanics of Materials 2, 123–137.

Li, D.S., Wisnom, M.R., 1996. Predicting transverse cracking in cross-ply laminates—an improved statistical approach. In: Proceedings of ECCM-7, Realising Their Commercial Potential, vol. 1. Woodhead Publishing Ltd, Abington Hall, Cambridge, U.K.

Nairn, J.A., 1989. The strain energy release rate of composite microcracking: a variational approach. Journal of Composite Materials 23, 1106–1129.

Nairn, J.A., Hu, S., 1994. Matrix microcracking. In: Talreja, R. (Ed.), Damage Mechanics of Composite Materials. Elsevier Science B.V., Amsterdam, The Netherlands, pp. 187–243.

O'Brien, T.K., 1993. Local delamination in laminates with angle ply matrix cracks, part II: Delamination fracture analysis and fatigue characterization. In: Stinchcomb, W.W., Ashbaugh, N.E. (Eds.), Composite Materials: Fatigue and Fracture, vol. 4, ASTM STP 1156. American Society for Testing and Materials, Philadelphia, PA, pp. 507–538.

Ogihara, S., Takeda, N., 1995. Interaction between transverse cracks and delamination during damage progress in CFRP cross-ply laminates. Composites Science and Technology 54, 395–404.

Parvizi, A., Bailey, J.E., 1978. On multiple transverse cracking in glass fibre epoxy cross-ply laminates. Journal of Materials Science 13, 2131–2136.

Parvizi, A., Garrett, K.W., Bailey, J.E., 1978. Constrained cracking in glass fibre-reinforced epoxy cross-ply laminates. Journal of Materials Science 13, 195–201.

Peters, P.W.M., 1984. The strength distribution of 90° plies in 0/90/0 graphite-epoxy laminates. Journal of Composite Materials 18, 545–556.

Prosser, W.H., Jackson, K.E., Kellas, S., Smith, B.T., McKeon, J., Friedman, A., 1995. Advanced waveform-based acoustic emission detection of matrix cracking in composites. Materials Evaluation, September, pp. 1052–1058.

Reifsnider, K.L., 1977. Some fundamental aspects of the fatigue and fracture response of composite materials. In: Proceedings of the 14th Annual Society of Engineering Science Meeting, Lehigh University, 14–16 November 1977, Bethlehem, PA, pp. 373–384.

Sendeckyj, G.P., Richardson, M.D., Pappas, J.E., 1974. Fracture behavior of Thornel 300/5208 graphite-epoxy laminates—Part 1: Unnotched laminates. In: Wu, E.M. (Ed.), Composite Reliability, ASTM STP 580. American Society for Testing and Materials, Philadelphia, PA, pp. 528–546.

Wang, A.S.D., 1984. Fracture mechanics of sublaminate cracks in composite materials. Composites Technology Review 6, 45–62.

Wang, A.S.D., Crossman, F.W., 1980. Initiation and growth of transverse cracks and edge delamination in composite laminates. Part 1. Energy method. Journal of Composite Materials Supplement 14, 71–87.

Xia, Z.C., Carr, R.R., Hutchinson, J.W., 1993. Transverse cracking in fiber-reinforced brittle matrix, cross-ply laminates. Acta Metallurgica et Materialia 41, 2365–2376.

Zang, W., Gudmundson, P., 1993. Damage evolution and thermoelastic properties of composite laminates. International Journal of Damage Mechanics 2, 290–308.